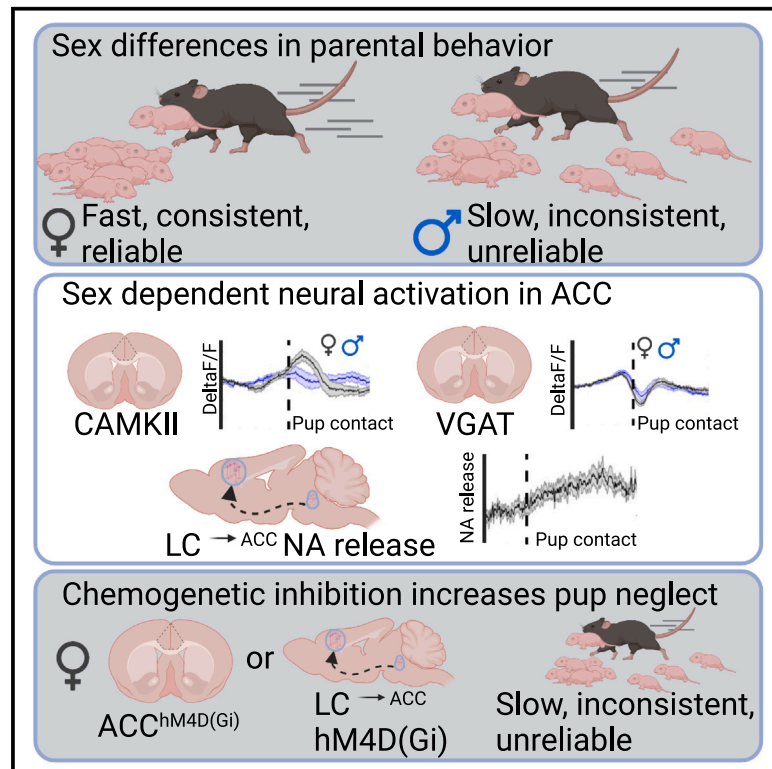# A circuit from the locus coeruleus to the anterior cingulate cortex modulates offspring interactions in mice

Graphical abstract

Authors

Alberto Corona, Jane Choe,
Rodrigo Muñoz-Castañeda, Pavel Osten,
Stephen D. Shea

Correspondence

sshea@cshl.edu

In brief

Corona et al. identify a noradrenergic pathway from locus coeruleus to cingulate cortex important for parental care. Using brain-wide activity mapping, fiber photometry, and chemogenetic inactivation, they show that sex-dependent activity in this pathway is important for maternal behavior and that noradrenaline modulates ACC's response to pup distress.

Highlights

- ACC is active during parental pup retrieval behavior in a sex-dependent manner

- Excitatory and inhibitory ACC neurons exhibit opposing activity during pup retrieval

- DREADD inactivation of excitatory ACC neurons increases parental neglect in dams

- Retrieval evokes NA release in ACC, and inactivating this input disrupts pup care

Article

A circuit from the locus coeruleus to the anterior cingulate cortex modulates offspring interactions in mice

Alberto Corona,[1,2,3] Jane Choe,[1] Rodrigo Muñoz-Castañeda,[1] Pavel Osten,[1] and Stephen D. Shea[1,4,*]

[1]Cold Spring Harbor Laboratory, Cold Spring Harbor, NY 11724, USA
[2]Cold Spring Harbor Laboratory School of Biological Sciences, Cold Spring Harbor Laboratory, Cold Spring Harbor, NY 11724, USA
[3]Present address: Icahn School of Medicine at Mount Sinai, New York, NY 10029, USA
[4]Lead contact
*Correspondence: sshea@cshl.edu
https://doi.org/10.1016/j.celrep.2023.112771

SUMMARY

Social sensitivity to other individuals in distress is crucial for survival. The anterior cingulate cortex (ACC) is a structure involved in making behavioral choices and is influenced by observed pain or distress. Nevertheless, our understanding of the neural circuitry underlying this sensitivity is incomplete. Here, we reveal unexpected sex-dependent activation of ACC when parental mice respond to distressed pups by returning them to the nest ("pup retrieval"). We observe sex differences in the interactions between excitatory and inhibitory ACC neurons during parental care, and inactivation of ACC excitatory neurons increased pup neglect. Locus coeruleus (LC) releases noradrenaline in ACC during pup retrieval, and inactivation of the LC-ACC pathway disrupts parental care. We conclude that ACC maintains sex-dependent sensitivity to pup distress under LC modulation. We propose that ACC's involvement in parenting presents an opportunity to identify neural circuits that support sensitivity to the emotional distress of others.

INTRODUCTION

The ability to detect when others are experiencing distress or danger, and to assist them, is a fundamental aspect of social behavior. However, the neural circuit substrates of such behavior and its evolutionary antecedents remain unclear. Parental care requires an organism to weigh its behavioral options in terms of their risk to itself and the potential benefits to another animal. Parenting offers little proximal benefit to caregivers, yet protecting endangered offspring is essential for the survival of the species.[1] This decision is often influenced by the sex of the parent. In many species, males and females display dramatic differences in parenting behaviors.[2] For instance, female mammals typically care for the offspring, whereas males are often aggressive toward the young (reviewed elsewhere[1–5]) with only 5%–10% of mammalian species exhibiting paternal care.[6]

Recent work on pro-social behaviors in rodents has opened the door to a better understanding of the neural circuit basis of social sensitivity to distress.[7–12] For example, the anterior cingulate cortex (ACC) responds to social information and the emotional state of others, especially distress.[7–12] ACC is implicated in social transfer of pain,[10] cost-benefit decision making,[13] observational fear learning,[7] and disrupted social interactions in the *Shank3* mouse model of autism.[14] With regard to parental behavior, ACC lesions in rats disrupt maternal behavior in early *post partum* days (PPDs),[15] and functional MRI (fMRI) studies

in humans show ACC is activated by infant cries.[16] Taken together, these data suggest that ACC regulates social cognition and may participate in computations that balance between the drive to help others and the drive to avoid danger and risk.

One potentially relevant input to ACC is locus coeruleus (LC), which consists of a bilateral pair of nuclei in the pons serving as nearly the sole source of noradrenaline (NA) for the brain. LC is an important regulator of stress, arousal, and state-dependent cognitive processes,[17,18] and it also has an established role in maternal behavior.[19] Mice lacking a gene necessary for NA synthesis exhibit deficits in maternal behavior, with most pups dying due to maternal neglect. This deficit is obviated by restoring NA signaling just before the birth of the pups.[19]

When mouse pups are separated from the nest, they emit ultrasonic distress vocalizations (USVs; 50–80 kHz). In response, the dam returns them to the nest in a behavior called pup retrieval.[20–25] We recently showed that a large fraction of LC neurons become robustly and precisely active as dams retrieve wayward pups and return them to the nest.[26] We proposed that LC contributes to goal-directed action selection during parenting with widespread release of NA.[26] However, the downstream targets through which LC modulates pup retrieval are unknown. ACC receives robust projections from LC,[27–29] and the activity in the two regions is highly correlated when external stimuli trigger phasic activation of LC.[30] Therefore, we hypothesized that LC influences ACC to regulate maternal care.

Although pup retrieval behavior has been observed in sires,[31–34] their behavior is less robust and consistent compared to dams. In particular, sires are slower at retrieving pups to the nest. We hypothesize that sires are less sensitive to offspring distress compared to dams. To investigate sex differences in neural circuits that control sensitivity to offspring distress, we compared how dams and sires respond to distressed pups. We used brain-wide imaging of the immediate-early gene *c-fos* to compare patterns of brain activity between retrieving and non-retrieving dams and sires. These experiments uncovered sex-dependent activation of ACC during interactions with pups. Fiber photometry recordings from parents actively engaged in pup retrieval corroborated this, revealing that excitatory and inhibitory neurons in ACC show stronger opposing patterns of activity during pup retrieval in dams as compared to sires. Chemogenetic inactivation of excitatory neurons in ACC increased the latency to retrieve pups and decreased parental interactions with distressed pups. We confirmed the reported existence of a projection from LC to ACC and found that phasic firing in LC evoked by pup retrieval triggered NA release in ACC. Finally, inactivating ACC inputs from LC increased parental neglect. Therefore, we propose that ACC adjusts parental sensitivity to pup distress through LC modulation in a sex-dependent manner.

RESULTS

Sex-dependent differences in pup retrieval behavior

While both sexes participated in parental care, we observed quantitative sex differences in interactions of CBA/CaJ parents with their pups. We quantified the efficacy of pup retrieval in the home cage (Figure 1A). Briefly, pups were scattered, and we calculated a normalized measure (ranging from 0 to 1) of the latency to return all pups to the nest (see STAR Methods).[35] Higher latency reflects poorer performance. Dams exhibited reliable retrieval on early trials and rapidly improved over time (Figures 1B–1F). In contrast, sires retrieved inconsistently and failed to improve as rapidly as dams, as evident from their higher mean retrieval latency scores (Figures 1B–1D). Previous work showed that sires of the ICR strain do not gather pups in a novel environment.[31] Therefore, we performed the retrieval assay in a novel cage to assess sex differences in contextual regulation of parental behavior. In the novel cage, sires exhibited significantly higher mean latencies and poorer day-to-day improvement, but this was not the case in dams (Figure 1C).

In both contexts, across PPD0–PPD5, sires retrieved fewer pups than dams (Figure 1I), and sires took longer than dams to initiate contact with the first pup (Figure 1J). The duration of individual retrieval events, measured as the time between pup contact and its deposition in the nest, did not differ between sires and dams (Figure 1K), demonstrating that sires and dams are equally capable of performing motor aspects of the behavior. However, the intervals between retrieval events were significantly longer in sires compared to dams (Figure 1L). Regardless of context, retrieval performance was significantly poorer in sires as compared to dams (Figure 1H).

We also observed that dams and sires are differentially sensitive to pups in distress. We transferred the pups to a glass jar with a lid with small holes in it, allowing access to sound and odor (not touch), and we placed it in the home cage. (Figure 1M; Videos S1 and S2). Being in the jar elicited overt signs of distress in the pups; the pups emitted significantly more USVs in the jar compared to when they were in the nest (Figure 1O). We recorded each animal's behavior in their home cage in the presence of a jar containing pups and in the presence of an empty jar; in both conditions, there were no pups outside the jar. Dams spent considerable time interacting with the sealed opening of the jar, including sniffing, biting, and clawing at the lid. The jar containing pups elicited a significantly greater investigatory response in the dams when compared to an empty jar or males with either jar (Figure 1N).

Brain-wide activity mapping reveals regions activated during pup retrieval

In addition to these expected behavioral differences, we found evidence for underlying sex differences in the brain-wide patterns of neural activation when parents interact with distressed pups. To identify regions that modulate parental interactions in dams and sires, we performed a brain-wide screen for differential expression of the immediate-early gene *c-fos* with an automated pipeline.[36] In short, *c-fos* expression was induced in dams and sires by one of several behavioral conditions. Ninety minutes later, subjects were sacrificed. Harvested brains were cleared, immunolabeled, and imaged with light-sheet microscopy. Custom software automatically registered the image stacks to a standardized atlas and counted *c-fos*$^+$ nuclei for 825 regions of interest (ROIs) (Tables S1–S3; Figures S1K–S1N).

We examined whole-brain *c-fos* expression patterns in mice exposed to one of four conditions: baseline, isolated, reunited with pups, and pup retrieval (Figure 2A). In dams, irrespective of ROIs, the baseline group showed significantly lower counts and less variability between individuals when compared to the isolated, reunion, and retrieval groups (Figure S1M). Sires showed greater overall variability in *c-fos*$^+$ cell counts, including baseline, and no significant differences across most of the groups (Figures S1N and S2E–S2H). Comparison of *c-fos* expression between the four experimental groups identified brain areas affected by the different behavioral conditions (Figures S1A–S1J) Therefore, *c-fos* expression patterns resulted from presence of the pups, absence of the pups, reunion with the pups, or retrieval of the pups.

The comparison between dams of the baseline group versus the retrieval group likely reflects changes in ROIs associated with pup retrieval. We identified ROIs that showed significantly different *c-fos* expression in the retrieval condition compared to all other control conditions and corrected for false discovery rate (Figure 2B). We observed increased *c-fos*$^+$ cell counts in the retrieval condition in ROIs that had been previously implicated in parenting. For example, we detected higher *c-fos*$^+$ cell counts in the bed nucleus of the stria terminalis (BNST)[37–41]; the medial hypothalamic zone, which includes the medial preoptic area, (MEZ)[32,33,42–46]; the medial septal complex (MSC)[47]; the basomedial amygdala (BMA)[48,49]; and the central amygdala (CEA).[50] In contrast to sires (Figure S2), most differences between the baseline and the retrieval groups in dams were increased *c-fos*$^+$ cells in mice from the retrieval group (Figure 2D), suggesting that the changes in *c-fos* were
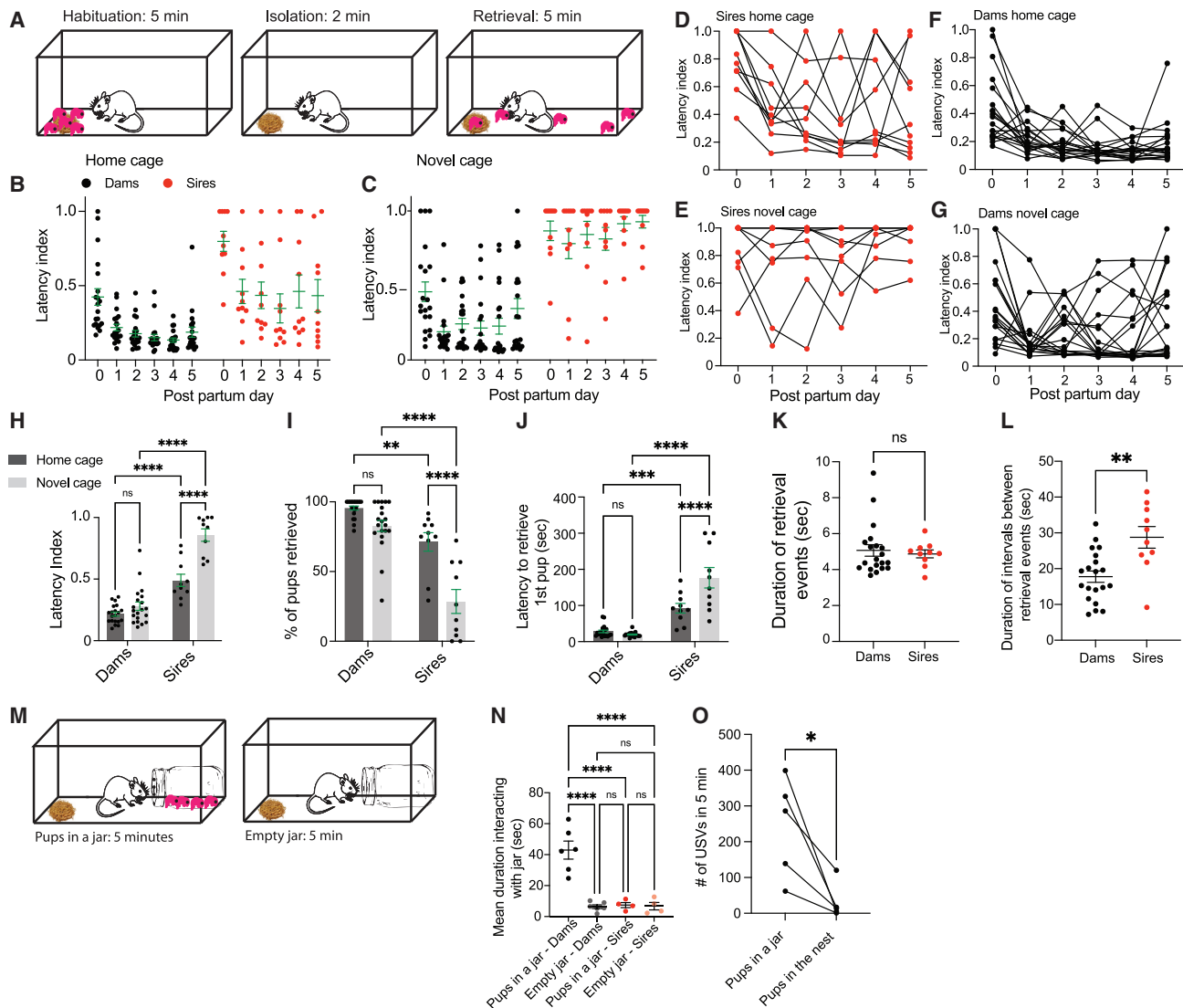
Figure 1. Sex-dependent differences in pup retrieval behavior

(A) Schematic of behavioral paradigm.

(B and C) Scatterplots showing a normalized measure of latency to gather pups for dams (n = 20) and sires (n = 10).

(D and E) Plot of retrieval latency of sires in the home and a novel cage, respectively. Lines track each individual's performance.

(F and G) Plot of retrieval latency of dams in the home and a novel cage, respectively. Lines track each individual's performance.

(H) Plot of mean latency index (PPD0–PPD5); n = 10 sires and 20 dams; two-way ANOVA; Holm-Sidak test, main factor (sex) p < 0.0001, main factor (context) p < 0.0001, interaction p = 0.0001; ****p < 0.0001.

(I) Plot of percentage of pups retrieved averaged across PPD0–PPD5; n = 10 sires and 20 dams; two-way ANOVA; Holm-Sidak test, main factor (sex) p < 0.0001, main factor (context) p < 0.0001, interaction p = 0.0031; ****p < 0.0001, **p = 0.0023.

(J) Plot of mean latency to retrieve the first pup (PPD0–PPD5); n = 10 sires and 20 dams; two-way ANOVA; Holm-Sidak test, main factor (sex) p < 0.0001, main factor (context) p = 0.0013, interaction p = 0.0001; ****p < 0.0001, ***p = 0.0003.

(K) Plot of mean duration of retrieval events in the home cage (n = 20 dams and n = 10 sires, unpaired t test, p = 0.6903).

(L) Plot of mean duration of intervals between retrieval events in the home cage (n = 20 dams and n = 10 sires, unpaired t test, **p = 0.0014).

(M) Schematic of jar behavioral paradigm.

(N) Plot of mean duration of time subjects interacted with pups in a jar and an empty jar (n = 6 dams and n = 4 sires; one-way ANOVA p < 0.0001; Tukey tests for individual group comparisons, ****p < 0.0001).

(O) Plot of the number of USVs emitted by the pups in the jar in the nest without the dam. Paired t test *p = 0.0262. All values are reported as mean ± SEM, and all error bars denote SEM.
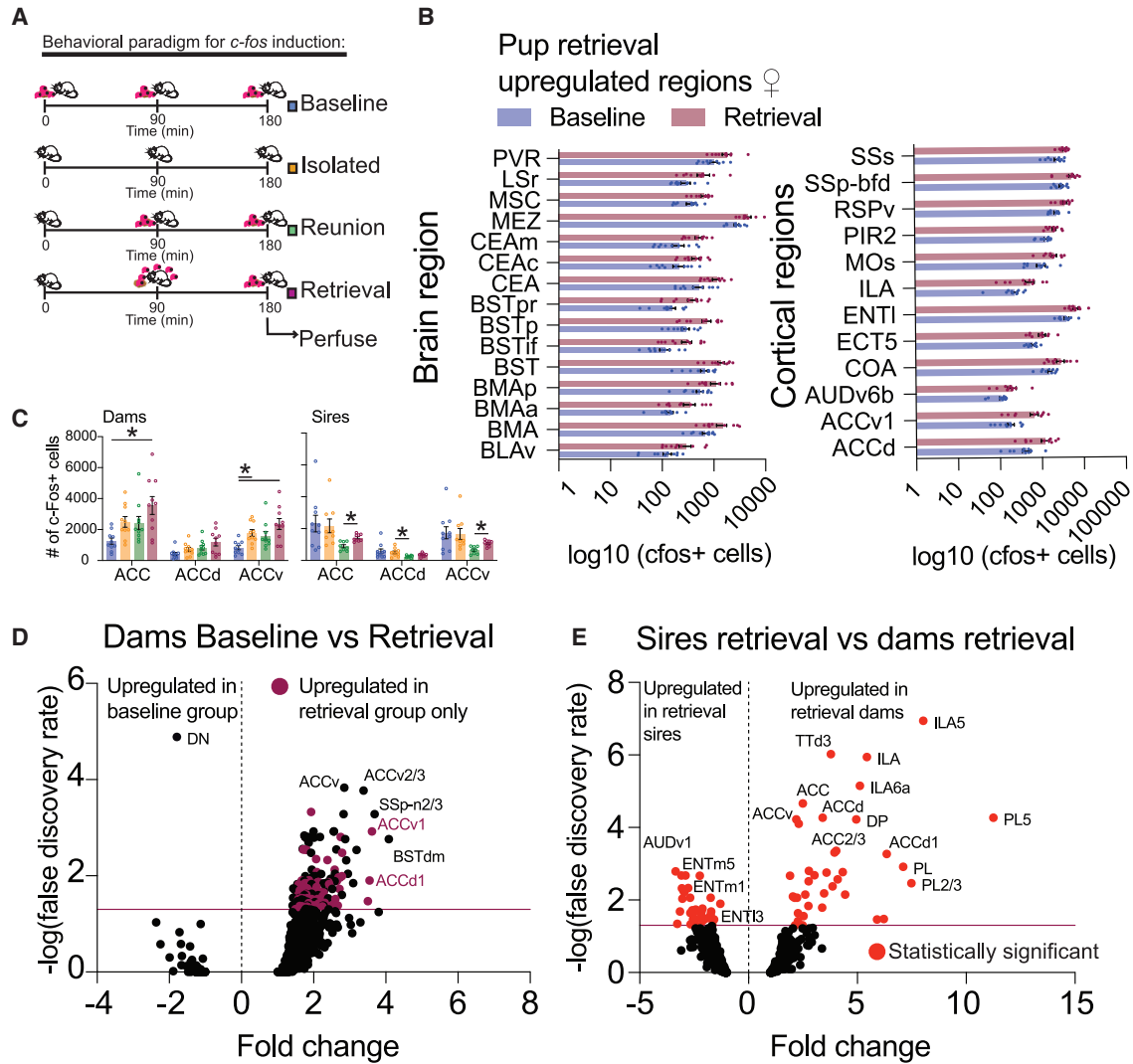
Figure 2. Brain-wide *c-fos* expression screen

(A) Schematic of behavioral protocol, performed in dams and sires (dams n = 10 per group; sires n = 10 baseline, nine isolated, eight reunion, and nine retrieval).

(B) Plots of brain regions in which *c-fos* expression was uniquely upregulated in the retrieval vs. baseline comparison in dams. PVR, periventricular region; LSr, lateral septal nucleus, rostral part; MSC, medial septal complex; MEZ, medial hypothalamic zone; CEAm, central amygdala, medial part; CEAc, central amygdala, capsular part; CEA, central amygdala; BSTpr, bed nucleus of the stria terminalis, posterior division, principal nucleus; BSTp, bed nucleus of the stria terminalis, posterior division; BSTif, bed nucleus of the stria terminalis, posterior division, interfascicular nucleus; BST, bed nucleus of the stria terminalis; BMAp, basomedial amygdalar nucleus, posterior part; BMAa, basomedial amygdalar nucleus, anterior part; BMA, basomedial amygdalar nucleus; BLAv, basolateral amygdalar nucleus, ventral part; SSs, supplemental somatosensory area; SSp-bfd, primary somatosensory area, barrel field; RSPv, retrosplenial area, ventral part; PIR2, piriform area, pyramidal layer; MOs, secondary motor area; ILA, infralimbic area; ENTl, entorhinal area, lateral part; ECT5, ectorhinal area/layer 5; COA, cortical amygdalar area; AUDv6b, ventral auditory area, layer 6b; ACCv1, anterior cingulate area, ventral part, layer 1; ACCd, anterior cingulate area, dorsal part.

(C) Plot of *c-fos*[+] cell count in ACC of dams and sires following pup interactions; Dams, mixed-effects model, factor (behavioral condition) $p < 0.0001$, factor (brain region) $p < 0.00001$; Tukey test, *$p < 0.05$. Sires, mixed-effects model, factor (behavioral condition) $p = 0.0022$, factor (brain region) $p < 0.00001$; Tukey test *$p < 0.05$.

(D) Volcano plot of *c-fos* induction in baseline vs. retrieval conditions in dams as fold change in *c-fos*^{+} cells by region. False discovery rate (FDR) analysis was performed by the Benjamini-Hochberg procedure. Purple data points denote unique significantly different ROIs when comparing baseline vs. retrieval groups only. The purple horizontal line indicates the significance threshold (FDR < 0.05).

(E) Volcano plot comparing retrieval groups between dams and sires. Positive fold change indicates an upregulation in dams and negative fold changes indicate an upregulation in sires. Significant data points are red. The purple horizontal line indicates the significance threshold (FDR < 0.05).

driven by pup retrieval. We then compared dams and sires from the retrieval groups and identified ROIs with significantly higher *c-fos*[+] cell counts in dams or sires. Brain areas upregu-lated in dams relative to sires were primarily regions in the pre-frontal cortex, including the infralimbic, prelimbic, and cingulate cortices (Figure 2E).
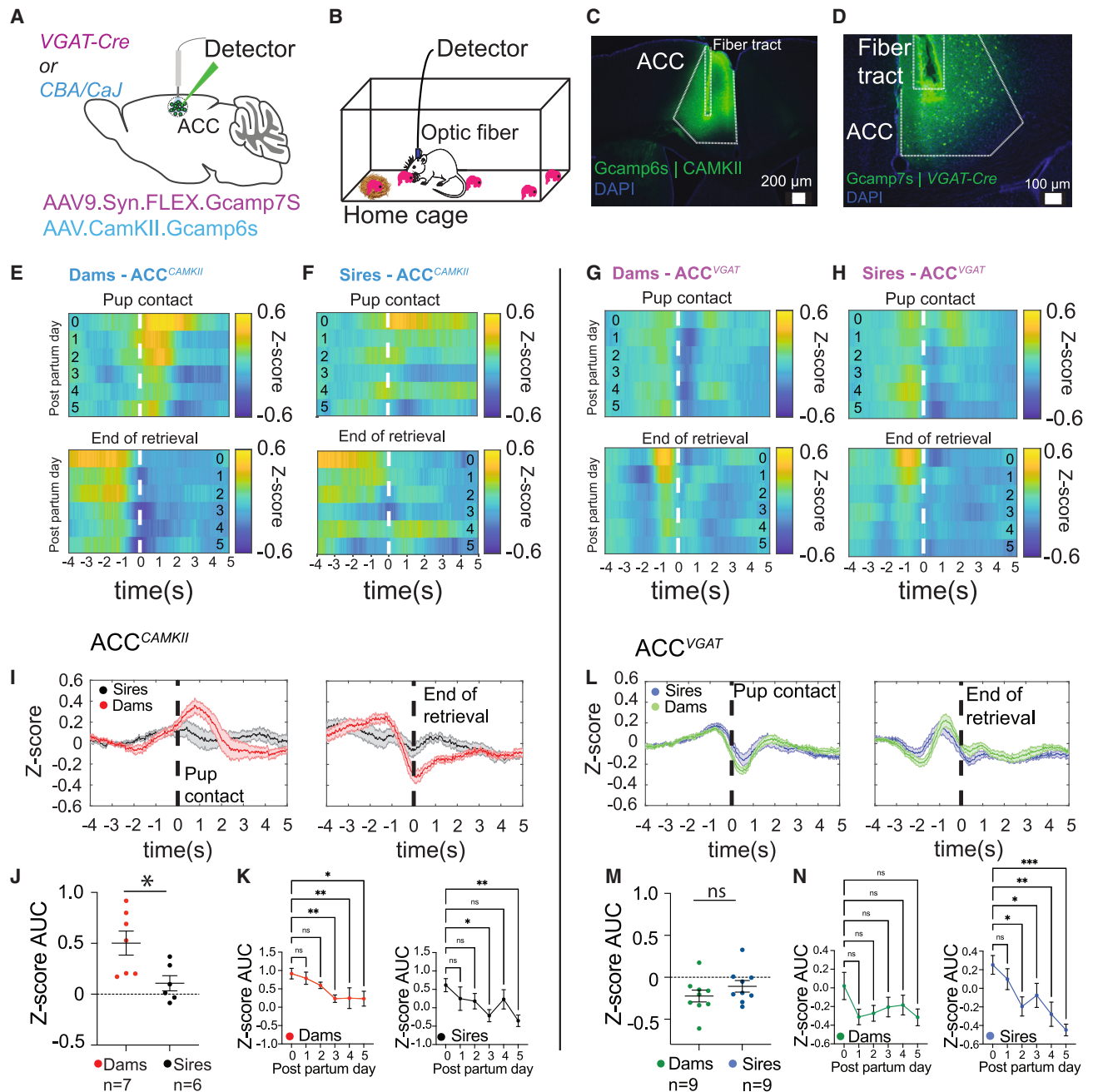
Figure 3. ACC^CAMKII but not ACC^VGAT neurons are differentially activated in dams and sires during pup retrieval behavior

(A) Schematic depicting our viral strategy to express GCaMP in excitatory and inhibitory neurons in ACC.

(B) Behavioral paradigm.

(C) Photomicrograph of a coronal brain section showing fiber placement and GCaMP6s expression in ACC^CAMKII neurons.

(D) Photomicrograph of a coronal brain section showing fiber placement and GCaMP7s expression in ACC^VGAT neurons.

(E) Heatmaps of mean GCaMP6s signals from ACC^CAMKII neurons during pup retrieval events in dams (n = 7). (Top) Heatmap aligned to pup contact. Each row is the mean activity of all mice by day. (Bottom) The same data aligned to the end of the retrieval events.

(F) Heatmaps of mean GCaMP6s signals from ACC^CAMKII neurons during pup retrieval events in sires (n = 6). Panels as in (E).

(G) Heatmaps of mean GCaMP7s signals from ACC^VGAT neurons during pup retrieval events in dams (n = 9). (Top) Heatmap of data aligned to pup contact. Each row is the mean activity of all mice by day. (Bottom) The same data aligned to the end of the retrieval events.

(H) Heatmaps of mean GCaMP7s signals from ACC^VGAT neurons during pup retrieval events in sires (n = 9). Panels are arranged as in (G).

(I) Plots of the mean Z-scored traces of ACC^CAMKII neurons for all mice and all days. Dams (red), sires (black).

(J) Comparison of the mean AUC of traces of retrieval-related activity of ACC^CAMKII neurons between dams and sires (Mann-Whitney U test, *p = 0.035).

(legend continued on next page)

One prominent unexpected region that captured our attention was ACC, which exhibited some of the largest *c-fos* upregulation in dams from baseline to retrieval (Figure 2D) and was upregulated in sires from reunion to retrieval (Figure 2C). Although ACC lesions impair maternal behavior in rats,[15] ACC is not widely appreciated as a major regulator of maternal behavior; the specific function and timing of its involvement in pup retrieval are unexplored. Moreover, ACC exhibited one of the largest disparities between dams and sires of all ROIs (dams > sires), potentially revealing sex-dependent modulation during interactions with pups (Figure 2E). We chose to focus the rest of this study on ACC because of the sex difference in *c-fos* activity, its unexpected involvement in parenting, its sensitivity to conspecific distress, and its ability to influence behavioral choices.

ACC^CAMKII but not ACC^VGAT neurons are differentially activated in dams and sires during pup retrieval

To more precisely observe the temporal relationship between ACC activity and interactions with pups, we performed fiber photometry in ACC of freely moving mice during pup retrieval (Figures 3A and 3B). We expressed GCaMP6s in ACC excitatory neurons (ACC^CAMKII) with an adeno-associated virus (AAV) containing the Ca^{2+}/Calmodulin-dependent protein kinase II (CAMKII) promoter (Figure 3C) and GCaMP7s in inhibitory neurons (ACC^VGAT) with a Cre-dependent AAV in vesicular GABA transporter Cre (VGAT-Cre) mice (Figure 3D). We recorded calcium activity from PPD0–PPD5 during interactions with pups. We found peaks of activity in ACC^CAMKII neurons locked to pup retrieval in dams and sires that decreased in magnitude over days (Figures 3E–3H). There was a significant sex difference in the magnitude of these calcium events, with dams showing stronger activation of ACC^CAMKII neurons during retrieval compared to sires (Figures 3I–3K). The decreasing magnitude of responses over days was not caused by degradation of the fluorescent signal. We separately expressed GCaMP6s in ACC^CAMKII in female mice and recorded the retrieval activity across two litters (Figure S3). As in the single-litter families, activity disappeared by PPD5 with the first litter; however, strong activity subsequently reappeared after the delivery of the second litter (Figure S3).

In contrast to ACC^CAMKII neurons, ACC^VGAT neurons showed an abrupt reduction in activity at pup contact followed by a peak of activity just before the end of each retrieval event (Figures 3G and 3H). We did not observe any significant sex-dependent differences in ACC^VGAT neuron activity during retrieval behavior (Figures 3L–3N). We confirmed the position of the optical fibers in ACC using immunohistochemistry (Figure S4).

We also observed sex differences in the relationship between ACC^CAMKII and ACC^VGAT neurons. The inverse relationship between the two cell types appeared to be weaker in sires compared to dams (Figure 4). In dams, activity of ACC^VGAT neurons was inversely related to that of ACC^CAMKII neurons during pup retrieval behavior (Figures 4B and 4C). We measured the magnitude of the responses as the area under the curve (AUC). After pup contact, ACC^CAMKII neurons increased their activity while ACC^VGAT neurons decreased their activity (Figure 4D). After the dams dropped the pups in the nest, this pattern reversed (Figure 4E).

ACC^VGAT neurons exhibited a sex-dependent decrease in activity when the dam entered the nest after all pups were retrieved. Activity returned to baseline level when the dam exited the nest (Figures 4F–4I). The activity of ACC^VGAT and ACC^CAMKII neurons was significantly different when the dams entered but not when they exited the nest (Figures 4J and 4K). Sires did not exhibit any significant differences between ACC^CAMKII and ACC^VGAT neurons during parenting (Figure 4L–4U). These data argue that there is sex-dependent involvement of ACC in pup retrieval and other parenting behaviors.

Silencing ACC^CAMKII neurons increases parental neglect

Based on these activity patterns during retrieval, we speculated that ACC^CAMKII neuron activity is necessary for attentive parenting in dams and sires. Therefore, we expressed either the inhibitory Designer Receptor Exclusively Activated by Designer Drugs (DREADDs) hM4D(Gi) or GFP in ACC^CAMKII neurons (Figure 5A), enabling us to silence ACC^CAMKII neurons with intraperitoneal (i.p.) injection of clozapine.[51,52] We confirmed selective expression of the inhibitory DREADDs in ACC using immunohistochemistry (Figures 5B, 5C, and S5). All mice were injected with clozapine or saline on alternating days according to the protocol depicted in Figure 5D. Chemogenetic inactivation of ACC^CAMKII neurons in dams disrupted pup retrieval behavior on early PPDs relative to GFP controls (Figures 5E and 5F). These results are consistent with our observation that ACC^CAMKII neurons are more strongly activated during pup retrieval on early PPDs (0–3) compared to later PPDs (4 or 5). These data suggest that ACC modulates retrieval behavior, particularly in the first few days after birth.

The same cohort was observed interacting with a jar containing pups or an empty jar 30 min after clozapine or saline injections (Figure 5D). Following clozapine injection, hM4D(Gi)-expressing dams spent significantly less time interacting with the jar of pups relative to GFP controls (Figure 5G) and relative to days when they were injected with saline (Figure 5K). There was no difference in this behavior between the hM4D(Gi) - and GFP-expressing dams when they were injected with saline (Figure 5H). No differences were observed between any of the groups in their behavior in the presence of an empty jar

---

(K) Comparison of the mean AUC of traces of retrieval-related activity of ACC^CAMKII neurons, showing a decline in the magnitude of activity over PPD0–PPD5. (Left) Dams' responses (Kruskal-Wallis test, **p = 0.0093; Benjamini, Krieger, and Yekutiel test, P0 vs. P3 **p = 0.0049; P0 vs. P4 **p = 0.0033; P0 vs. P5 *p = 0.0209). (Right) Sires' responses (Kruskal-Wallis test *p = 0.0433; Benjamini, Krieger, and Yekutieli test, P0 vs. P3 *p = 0.0083; P0 vs. P5 **p = 0.0030).
(L) Plots of the mean traces of ACC^VGAT neurons for all mice and all days comparing dams (green) and sires (blue).
(M) Comparison of the mean AUC of traces of retrieval-related activity of inhibitory neurons between dams and sires. (Mann-Whitney test, p = 0.3401).
(N) Comparison of the mean AUC of traces of retrieval-related activity of ACC^VGAT neurons, showing a decline in the magnitude of activity over PPD0–PPD5. (Left) Dams' responses (Kruskal-Wallis test, not significant [n.s.], p = 0.2914). (Right) Sires' responses (Kruskal-Wallis test ***p = 0.0008; Benjamini, Krieger, and Yekutieli test P0 vs. P2 *p = 0.0228; P0 vs. P3 *p = 0.0571; P0 vs. P4 **p = 0.0020; P0 vs. P5 ***p < 0.0001).
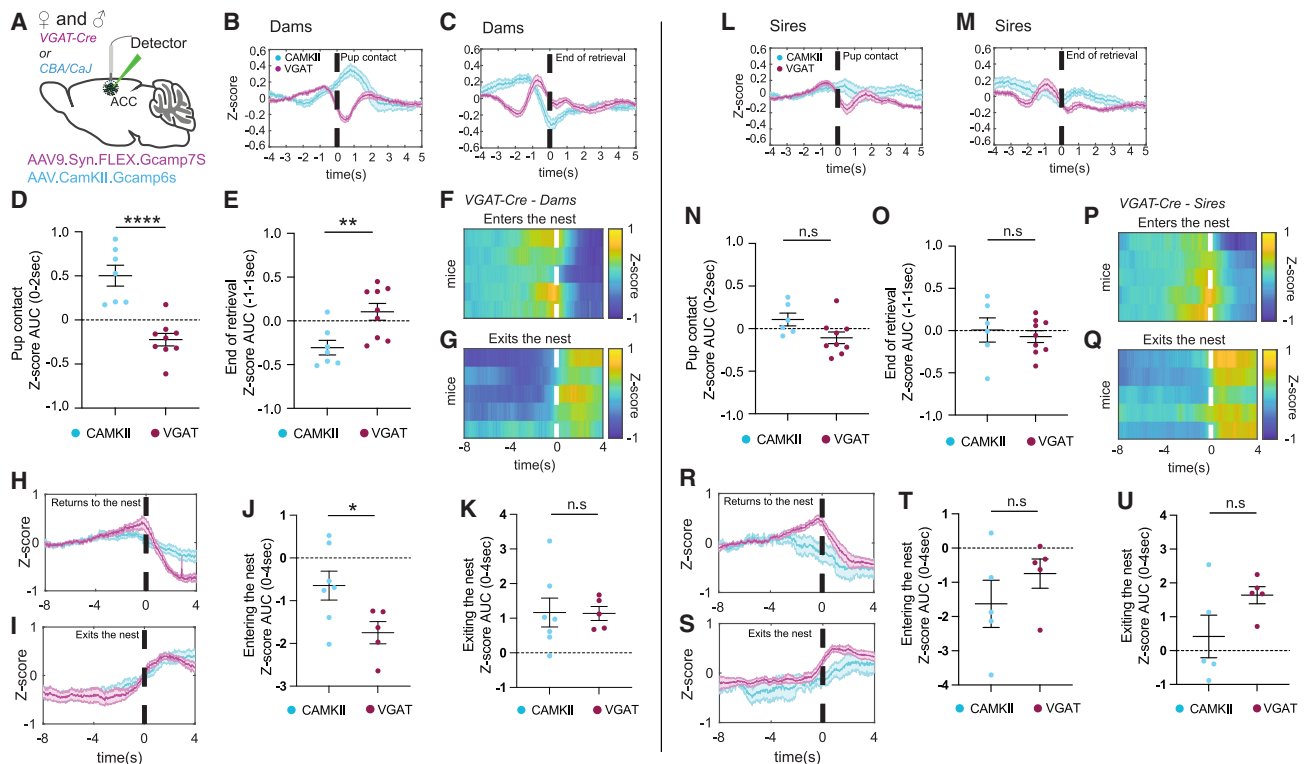
Figure 4. ACC^CAMKII and ACC^VGAT cell populations show opposite activation patterns during pup retrieval in dams but not sires

(A) Schematic depicting our viral strategy to express GCaMP in ACC^VGAT and ACC^CAMKII neurons.

(B and C) Plots of the mean traces of ACC^CAMKII neurons (cyan) and ACC^VGAT neurons (magenta) during pup retrieval for all dams and all days (n = 7 mice and n = 9 mice respectively). Plot in (C) is aligned to the end of the retrieval events.

(D and E) Comparison of the mean AUC of traces of retrieval-related activity between ACC^CAMKII neurons and ACC^VGAT neurons in dams, aligned to pup contact (unpaired t test ****p < 0.0001) (D) and the end of retrieval (unpaired t test **p = 0.0074) (E).

(F and G) Heatmaps of mean GCaMP7s signals from ACC^VGAT neurons in dams. Signals are aligned to the entry of the dam to the nest (F) and the exit of the dam from the nest (G) after retrieval of all pups. Each row represents the mean Z score from PPD0–PPD5 for each mouse (n = 5 mice).

(H and I) Plots of the mean traces of ACC^CAMKII neurons (cyan) and ACC^VGAT neurons (magenta) for all dams and all days aligned to the dams' entry to the nest (H) and exit from the nest (I) (n = 5 mice).

(J and K) Comparison of the mean AUC of traces of nest entry/exit-related activity between ACC^CAMKII neurons and ACC^VGAT neurons in dams, aligned to the dam entering the nest (unpaired t test *p = 0.0378) (J) and exiting the nest (K) (unpaired t test n.s. [p = 0.9613]).

(L and M) Plot of the mean traces of ACC^CAMKII neurons (cyan) and ACC^VGAT neurons (magenta) for all sires and all days (n = 6 mice and n = 9 mice respectively) aligned to pup contact during pup retrieval (L) and the end of the retrieval events (K).

(N and O) Comparison of the mean AUC of traces of retrieval-related activity between ACC^CAMKII neurons and ACC^VGAT neurons in sires from all days aligned to pup contact (unpaired t test, n.s. [p = 0.0581]) (N) and to the end of retrieval (unpaired t test, n.s. [p = 0.5936]) (O).

(P and Q) Heatmaps of mean GCaMP7s signals from ACC^VGAT neurons in sires. The signals are aligned to the sire's entry (P) and exit (Q) from the nest after retrieval of all pups. Each row represents the mean Z score from PPD0–PPD5 for each mouse (n = 5 mice).

(R and S) Plots of the mean traces of ACC^CAMKII (cyan) and ACC^VGAT neurons (magenta) for all sires and all days aligned to the sire's entry (R) and exit (S) from the nest (n = 5 mice).

(T and U) Comparison of the mean AUC of traces of nest entry/exit-related activity between ACC^CAMKII and ACC^VGAT neurons in sires from all days aligned to the sires' entry (unpaired t test, n.s. [p = 0.3085]) (T) and exit from the nest (unpaired t test, n.s [p = 0.1092]) (U).

(Figures 5I, 5J, and 5L). These results show that silencing ACC^CAMKII neurons in dams increases pup neglect and may also decrease maternal motivation.

We used the same strategy to assess the consequences of inactivating ACC^CAMKII neurons in sires. Chemogenetic inactivation of ACC^CAMKII neurons in sires does not significantly disrupt pup retrieval (Figures 5M and 5N). However, inactivation of ACC^CAMKII neurons on PPD0 affected pup retrieval performance on subsequent days such that hM4D(Gi)-expressing sires appear to be impaired even after a saline injection (Figures 5M

and 5N). With regard to trapped pups, all sires spent significantly less time than dams interacting with a jar containing pups, but they did not differ from dams in their interactions with an empty jar. hM4D(Gi)-expressing sires spent less time interacting with the pups in the jar than GFP controls when injected with clozapine (Figure 5O) and not when injected with saline (Figure 5P). We found no significant differences in the time spent interacting with an empty jar between hM4D(Gi)-expressing mice and GFP controls injected with clozapine or saline (Figures 5Q and 5R). Chemogenetic inactivation of ACC^CAMKII neurons did not affect
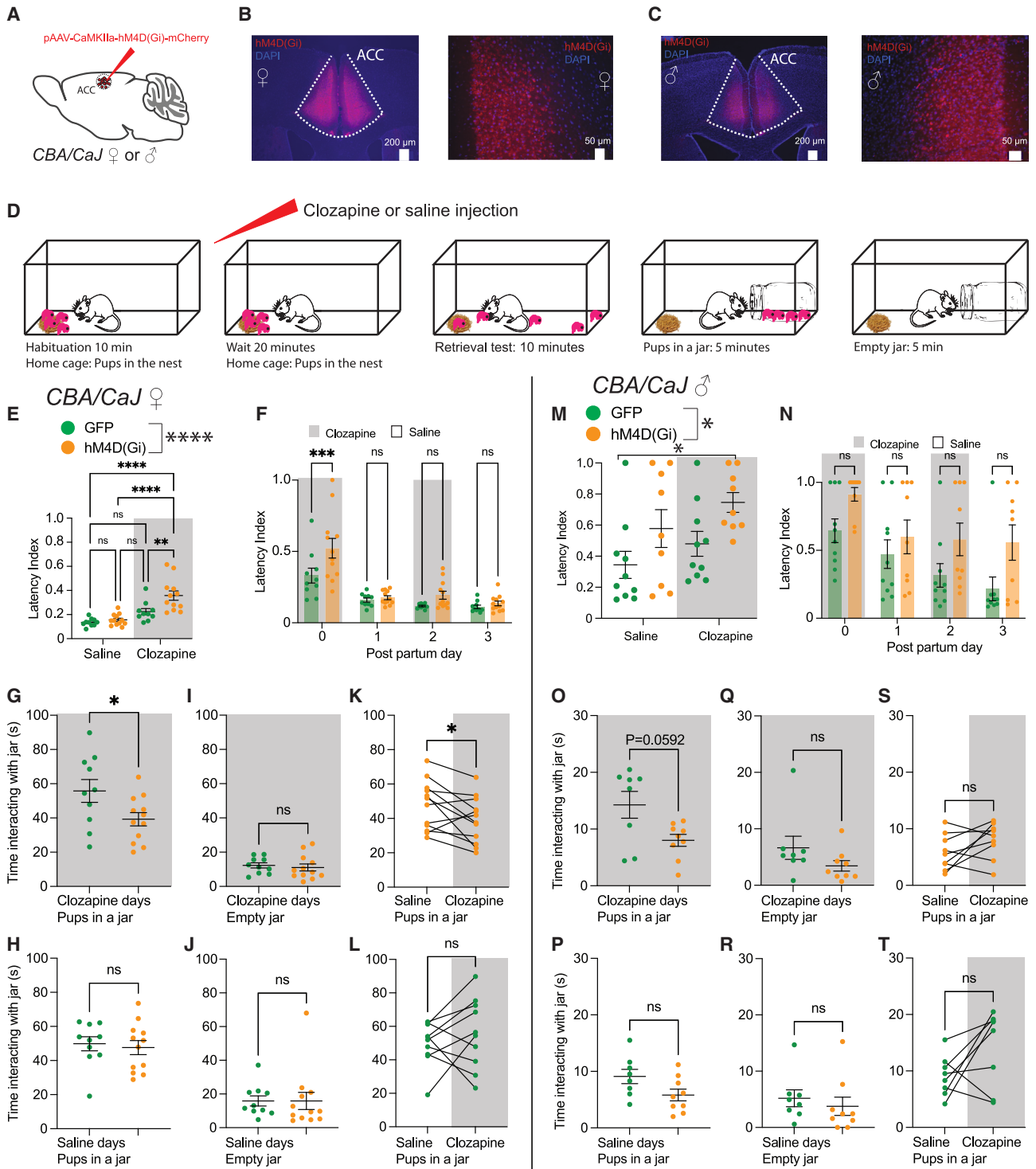
Figure 5. Chemogenetic inactivation of ACC^CAMKII neurons disrupts pup-directed behaviors

(A) Schematic of the viral strategy used to inactivate ACC^CAMKII neurons.

(B and C) Photomicrographs of hM4D(Gi) expression in ACC.

(D) Behavioral paradigm.

(E) Scatterplot of mean latency index (±SEM) in GFP-expressing dams (green) injected with saline or clozapine (n = 10), and hM4D(Gi)-expressing dams (orange) injected with saline or clozapine (n = 12), one-way ANOVA, ****p < 0.0001; Tukey test, **p = 0.0039, ****p < 0.0001.

(legend continued on next page)

sires' behavior when comparing hM4D(Gi)-expressing mice injected with clozapine or saline (Figure 5S). Collectively, our chemogenetic data show that inactivation of ACC[CAMKII] neurons increases pup neglect and decreases sensitivity to respond to pup distress in dams and not in sires.

Importantly, the effect on behavior that we observed from inactivating ACC[CAMKII] neurons was not due to a direct effect on anxiety-like behaviors. We tested hM4D(Gi)-expressing and GFP-expressing dams and sires injected with clozapine on an elevated-plus maze (Figures S6A and S6B). We found no significant differences in the percentage of time animals spent in the open arms (Figures S6C and S6E) or the number of entries to the open arms (Figures S6D and S6F).

Sex-dependent signaling from LC to ACC during pup retrieval

Previous reports have described ACC's afferents[29] and efferents.[53] Interestingly, ACC is interconnected with the noradrenergic LC,[29,53,54] and activity patterns in ACC and LC are coordinated.[30] The LC axons that impinge on ACC reportedly target excitatory neurons in ACC, not inhibitory neurons.[54] Previously we proposed that LC contributes to goal-directed action selection during parental behavior with global release of NA.[26] However, the downstream targets of LC that modulate social behavior according to NA signaling remain unknown. Therefore, we injected retrograde AAV (rAAV) in ACC as a sensitive retrograde tracer and confirmed a projection from LC to ACC (Figure 6A).

We then performed fiber photometry in LC of freely behaving dams and sires by injecting AAV driving Cre-dependent expression of GCaMP7s in LC of dopamine beta hydroxylase Cre (DBH-Cre) mice (Figure 6B). Pup retrieval responses in LC were longer in sires compared to dams (Figures 6C–6E). These responses were sustained for the entire pup retrieval event and returned to baseline activity levels when the mouse dropped the pup in the nest (Figure 6E). The AUC of LC responses (0 to +4 s relative to retrieval onset) were weaker in dams compared to sires (Figure 6F). Over all days, retrieval events were longer in sires (3.77 ± 0.04 s) than in dams

(3.15 ± 0.03 s) (Figure 6G), and sires had significantly longer intervals between retrieval events (sires, 20.37 ± 1.86 s; dams, 4.1 ± 0.31 s) (Figure 6H). Not surprisingly, the magnitude of LC responses was positively correlated with the duration of retrieval events (Figures 6I and 6J). Interestingly, the magnitude of the LC response and the time since the preceding retrieval event were also positively correlated (Figures 6K and 6L). We conclude that the temporal precision of the neural activity in LC reflects sex differences in the temporal precision of pup retrieval.

The high amplitude of phasic activity in LC during pup retrieval implies that the activity is pervasive through most LC neurons.[26] Neurons in LC that project to ACC (LC-ACC) share this phasic activity pattern. We injected an rAAV in ACC to express Cre recombinase in LC-ACC, and we injected Cre-dependent GCaMP7s AAV in LC (Figures 7A and 7B). We found that 82.2% ± 4.1% of GCaMP7s⁺ cells co-express tyrosine hydroxylase (TH). Indeed, during pup retrieval, LC-ACC neurons exhibited temporally precise calcium transients time locked to pup contact that were similar to those seen in recordings from all neurons in LC (Figures 7C–7E). Calcium activity of ACC-projecting LC neurons was correlated with behavioral metrics (duration of retrieval events and intervals between retrieval events) in most mice (Figure 7F–7H). These events likely resulted in NA release in ACC during pup retrieval. We injected a GRAB_NE sensor[55] in ACC, and we observed NA release associated with pup retrieval (Figures 7I–7L). Comparing the AUC of the NA signal at baseline to the AUC after pup contact, there was a significant rise in NA release during pup retrieval relative to baseline (Figure 7K). We confirmed the position of the optical fibers above LC using immunohistochemistry (Figure S7). These data establish a functional connection between LC and ACC associated with parental behavior.

Selectively silencing noradrenergic input to the ACC impairs pup retrieval

Finally, we tested whether the LC-ACC circuit is necessary for parental behavior. We injected an rAAV in ACC to express Cre

---

(F) Scatterplot of the data in (E), separated by day. Two-way ANOVA with Sidak test, main effect (day ****p < 0.0001, main effect (virus) **p = 0.0025, interaction p = 0.05, ***p = 0.0009.

(G and H) Plots comparing time interacting with the trapped pups for GFP-expressing dams (green, n = 10) and hM4D(Gi)-expressing dams (orange, n = 12) injected with clozapine (G) (Mann-Whitney test, *p = 0.0426) and injected with saline (H) (Mann-Whitney test, p = 0.6277).

(I and J) Plots comparing time interacting with the empty jar for GFP-expressing dams (green; n = 10) and hM4D(Gi)-expressing dams (orange, n = 12) injected with clozapine (I) (Mann-Whitney test, p = 0.4176) and injected with saline (J) (Mann-Whitney test, p = 0.3463).

(K) Plot comparing time interacting with the trapped pups by hM4D(Gi)-expressing dams injected with saline or clozapine (n = 12) (paired t test, *p = 0.0369).

(L) Plot comparing time interacting with the trapped pups by GFP-expressing dams injected with saline or clozapine (n = 10) (paired t test, p = 0.4038).

(M) Scatterplot of mean latency index (±SEM) in the same GFP-expressing sires (n = 10, green) when injected with saline or clozapine, and the same hM4D(Gi)-expressing sires (n = 9, orange) when injected with saline or clozapine; one-way ANOVA, *p = 0.02; Tukey test, asterisk indicates significant differences, *p = 0.0168.

(N) Scatterplot of the data in (M) separated by day. Two-way ANOVA with Sidak test, main effect (day) **p = 0.0014, main effect (virus) ***p = 0.0008, interaction p = 0.7601.

(O and P) Plot comparing time interacting with the trapped pups for GFP-expressing sires (n = 8) and hM4D(Gi)-expressing sires (n = 9) injected with clozapine (O) (Mann-Whitney test, p = 0.0592) and injected with saline (P) (Mann-Whitney test, n.s.).

(Q and R) Plot comparing time interacting with the empty jar for GFP-expressing sires (n = 8) and hM4D(Gi)-expressing sires (n = 9) injected with clozapine (Q) and saline (R) (Mann-Whitney test, n.s.).

(S) Plot comparing time interacting with the trapped pups by hM4D(Gi)-expressing sires injected with saline or clozapine (n = 9), (paired t test, p = 0.1392).

(T) Plot comparing time spent interacting with the trapped pups for GFP-expressing sires injected with saline or clozapine (n = 8) (paired t test, p = 0.1024).
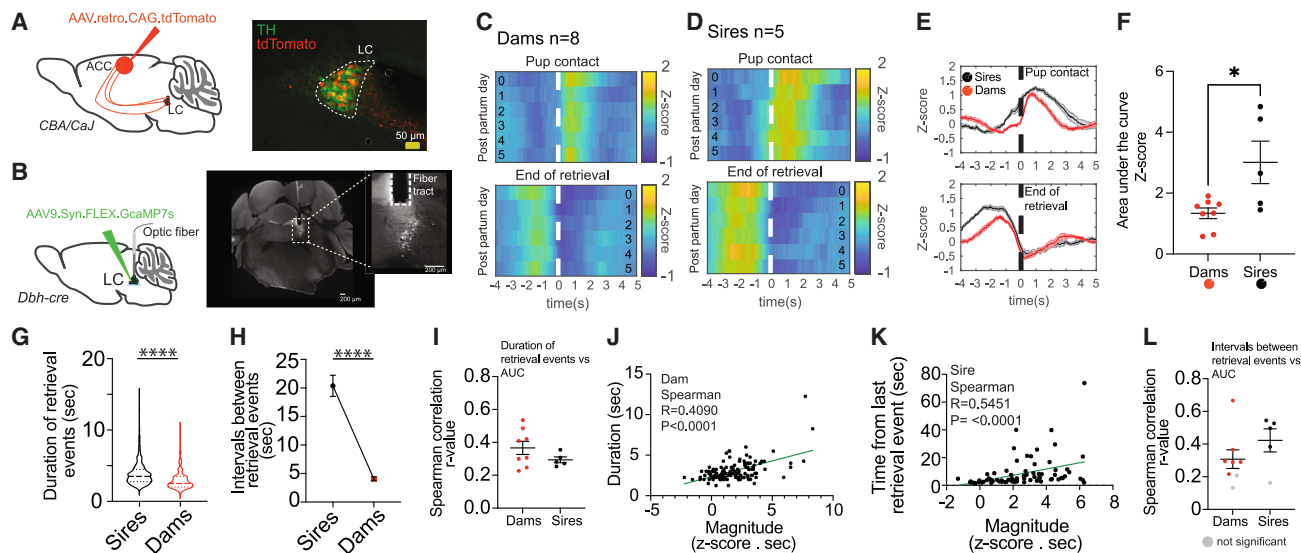
Figure 6. Timing and magnitude of LC activity associated with pup retrieval behavior is different in sires compared to dams

(A) Schematic of virus injection (left). Photomicrograph of a coronal brain section showing retrograde labeling from ACC to LC (right). Green shows tyrosine hydroxylase (TH) antibody staining and red shows tdTomato expression driven by the rAAV injection.

(B) Schematic of our viral strategy for expressing GCaMP7s in LC[DBH] neurons (left). Photomicrograph of a coronal brain section showing GCaMP7s expression in the LC (right). The placement of the optical fiber is also visible (inset).

(C and D) Heatmaps of mean GCaMP7 signals from LC during pup retrieval events in dams (n = 8 mice) (C) and sires (n = 5 mice) (D). Each row is the mean activity for all mice by day. (Top) Data aligned to pup contact. (Bottom) Data aligned to the end of retrieval.

(E) Plot of the mean traces of GCaMP7 signals in LC for all mice and all days, contrasting dams (red) and sires (black). (Top) Data aligned to pup contact. (Bottom) Data aligned to the end of the retrieval.

(F) Comparison of the mean AUC of traces of the retrieval-related activity of LC[DBH] neurons in dams and sires aligned to pup contact (Mann-Whitney test, p = 0.0451).

(G) Violin plots comparing the duration of retrieval events between dams and sires (sires n = 5 mice, 618 events; dams n = 8 mice, 1,238 events; Mann-Whitney test, p < 0.0001).

(H) Plot showing the duration of intervals in between retrieval events (n = 5 sires, n = 508 events; n = 8 dams, n = 1072 events; Mann-Whitney test, p < 0.0001).

(I) Scatterplot of coefficients (r) obtained from Spearman correlation of the duration of the retrieval events and the magnitude of LC responses during pup retrieval.

(J) Example scatterplot of the duration of retrieval events and the magnitude of LC responses in a dam. The green line represents a linear regression.

(K) Example scatterplot of the time between retrieval events and the magnitude of LC responses in a sire. The green line represents a linear regression.

(L) Scatterplot of coefficients (r) obtained from Spearman correlation of the intervals between retrieval events and the magnitude of LC responses during pup retrieval for all mice. Gray dots represent correlations that were not significant.

recombinase in LC-ACC neurons and Cre-dependent hM4D(Gi) in LC (Figures 7M and 7O). We found that 87% ± 2.4% of hM4D(Gi)+ cells co-express TH. We recorded interactions with pups 20 min after clozapine injection on PPD0–PPD3 (Figure 7N). Chemogenetic inactivation of LC-ACC neurons disrupted pup retrieval in early PPDs (Figure 7P). Although the inactivation of the LC-ACC circuit did not abolish pup retrieval behavior completely, it increased pup neglect and retrieval latency in dams.

DISCUSSION

Empathy can be defined as the adoption of another individual's emotional state. Rodents exhibit empathy-like behaviors such as vicarious fear learning,[7] social transfer of pain and analgesia,[10] and pro-social behaviors such as consolation.[8,11] ACC has been identified as a hub for information about the emotional state of others.[7,10] Here, we propose that the involvement of ACC in parental behavior presents a tractable model to reveal the neural computations that underlie decisions influenced by the social perception of distress. During parental encounters, adults need

to process offspring cues, including distress cues, and then select an appropriate behavioral response. We propose that ACC, in coordination with the noradrenergic LC, integrates distress signals from the offspring to promote a protective response.

Not surprisingly, our data show that paternal behavior is more variable and less robust than maternal behavior, consistent with previous reports. For instance, paternal but not maternal behavior is disrupted by the loss of oxytocin,[56] and disrupting prolactin signaling in the medial preoptic nucleus impairs paternal behavior.[34] One possibility for the observed behavioral variability is that males are more sensitive than females to contextual changes.[31] Most males did not retrieve pups in a novel environment, whereas the behavior of dams was not significantly altered in an unfamiliar context. These results suggest that paternal behavior is subject to greater contextual regulation than maternal behavior and reveal differential sensitivity to pup distress in dams and sires.

The neural substrates for behavioral choices during pro-social behaviors remain elusive. Using an unbiased brain-wide activity
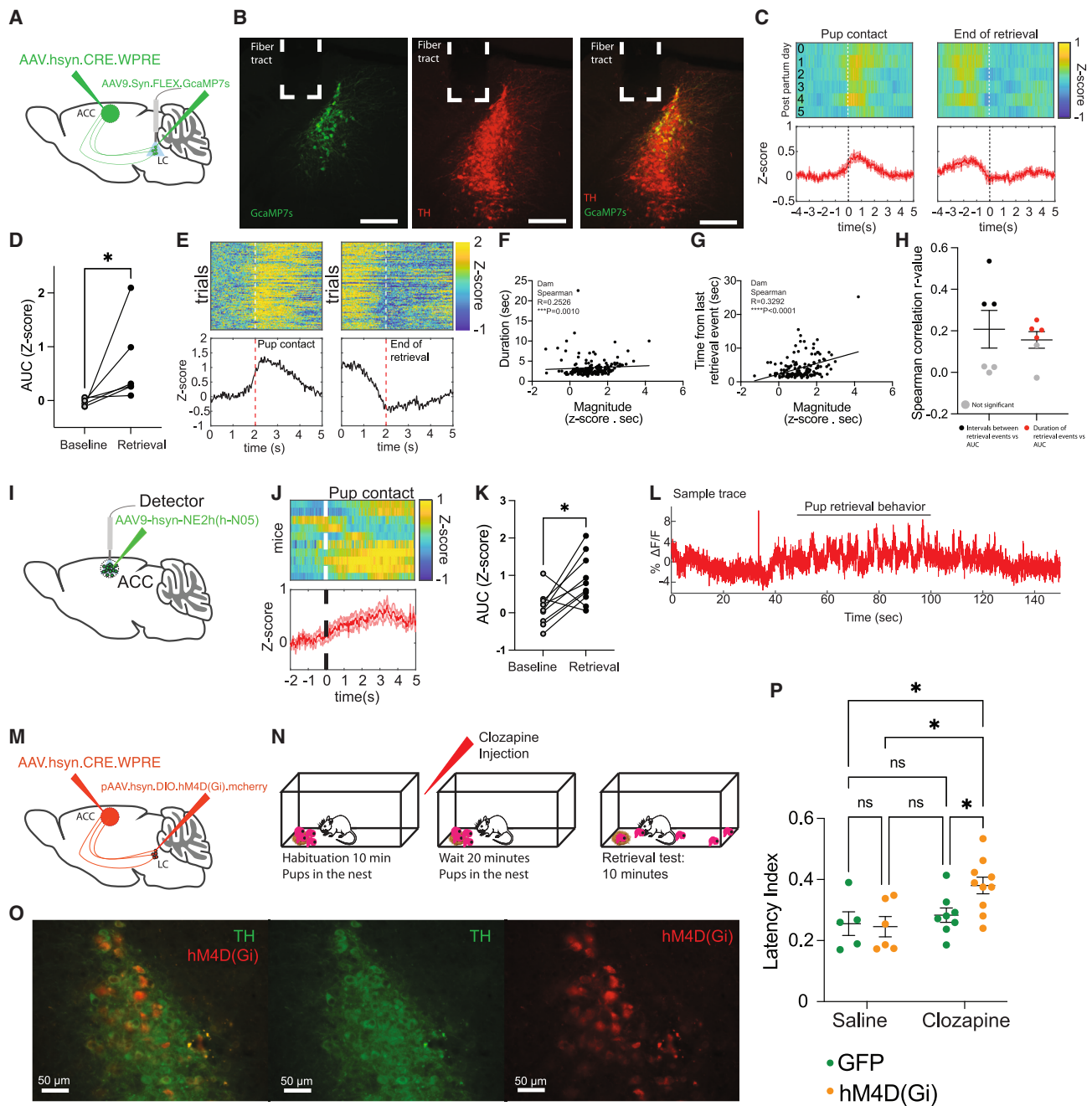
Figure 7. LC-ACC neurons are active during pup retrieval behavior, release NA in ACC, and selective inactivation of LC-ACC neurons disrupts pup retrieval behavior

(A) Schematic of our viral strategy for expressing GCaMP7s in LC neurons that project to ACC.

(B) Photomicrographs of a coronal brain section showing GCaMP7s expression (green), tyrosine hydroxylase (TH) antibody staining (red), and fiber placement in LC.

(C) Plots of activity of LC-ACC neurons during pup retrieval. The left panel shows a heatmap (top), wherein each row is the mean activity for all mice by day, and a plot (bottom) of mean GCaMP7s traces from LC-ACC neurons for all mice and all days. Data are aligned to pup contact. The right panel is the same data aligned to the end of retrieval.

(D) Plot of the mean AUC of the traces of retrieval-related activity of LC-ACC aligned to pup contact compared with baseline activity (Wilcoxon matched-pairs signed rank test, *p = 0.0312).

(E) Plots of activity from LC-ACC neurons during retrieval from one representative dam, arranged as in (C).

(F) Example scatterplot of the duration of retrieval events and the magnitude of LC-ACC responses in a dam. The black line represents a linear regression.

(G) Example scatterplot of the time between retrieval events and the magnitude of LC-ACC responses in a dam. The black line represents a linear regression.

(legend continued on next page)

screen, we associated ACC with parental behavior (Figure 2). We also observed sex-dependent ACC activation patterns in dams and sires that retrieve pups to the nest. Consistent with the behavioral variability observed in sires, *c-fos* expression levels were more variable in sires compared to dams. However, there are two limitations of immediate-early gene screens: first, they only provide a snapshot of brain activity from a given time window, and, second, they lack cell type specificity. To overcome these limitations, we directly observed the temporal dynamics of inhibitory and excitatory ACC neurons in freely moving mice during parenting.

Consistent with the higher expression levels of *c-fos* in ACC in dams compared to sires, our photometry results showed stronger activation of ACC[CAMKII] neurons in dams as compared to sires during pup retrieval (Figure 3). Neural responses in ACC during pup retrieval were stronger in early PPDs, presumably when the pups are more vulnerable to environmental conditions, and the behavior is being actively learned. Responses during pup retrieval start before the animals contact a pup prior to retrieving it to the nest. This suggests that the ACC[CAMKII] responses are associated with the late pre-execution stages of pup retrieval. We propose that ACC is involved in processing pup distress to influence engagement with the pups. It is possible that some input(s) to ACC may put the animal in a vigilant state during interactions with pups in distress by slowly affecting the excitability of ACC neurons, raising or lowering the threshold for making a decision. The differences in ACC[CAMKII] neural activity between dams and sires may contribute to differential behavioral sensitivity to pup distress.

Interactions between inhibitory and excitatory neural populations is essential for cortical processing.[57] We recorded the dynamics of inhibitory and excitatory neurons in ACC during pup retrieval (Figure 4). Interestingly, we observed an inverse relationship between ACC[CAMKII] and ACC[VGAT] cells in dams but not in sires. These data suggest that synaptic interactions between excitatory and inhibitory neurons in ACC may be weaker in sires compared to dams. Inhibitory neurons in ACC exhibit an abrupt decrease in activity when the mice enter the nest with pups and rapidly return to baseline when they exit. It is unclear what sensory attributes of the nest trigger this response. The role of ACC in parental decision making lacks a detailed description of the contribution of different cell types, so a natural extension of this work is to investigate the contribu-

tion of different types of excitatory (e.g., Fezf2, PlexinD1), inhibitory (e.g., parvalbumin-, somatostatin-, or vasoactive intestinal peptide-expressing), or projection neurons in ACC during free interactions with pups.

Inactivation of ACC impairs observational fear learning,[7] disrupts processing of observed pain,[10] and, in rats, impairs maternal behavior.[15] We hypothesized that ACC processes distress signals from the pups, and we predicted that inactivating ACC[CAMKII] neurons disrupts retrieval. Indeed, chemogenetic inactivation of ACC[CAMKII] neurons increased the latency to retrieve pups in early PPDs, but performance recovered as the pups got older (Figure 5). This is consistent with our photometry data that show stronger ACC activation during pup retrieval in early PPDs (Figure 3). We speculate that parents are more vigilant with young pups that are more susceptible to distress.

ACC receives inputs from many brain regions, including the noradrenergic LC.[28,29,54] LC plays an important role in arousal, stress, attention, and goal-directed action selection among many other functions (reviewed in Poe et al. and Ross and Van Bockstaele[58,59]). However, the mechanisms by which the noradrenergic system regulates socially motivated behavior and social distress remain poorly understood. LC modulates stress responses through corticotropin-releasing factor (CRF), which increases tonic firing in LC.[18] Interestingly, there is sex-dependent sensitivity to CRF in LC neurons, with female LC neurons being more sensitive to CRF compared to male LC neurons.[60] Thus, LC is a candidate region to modulate sex-dependent stress responses through its projections to ACC and influence parental behavior in response to pup distress. LC responses during pup retrieval were longer in sires compared to dams and reflected the temporal precision of the behavior. The fact that the sex difference in LC retrieval activity consists of larger responses in sires is surprising. One possible resolution to this apparent paradox could be additional sex differences in the response of ACC to NA. Future work on this circuit may resolve this issue. Altogether, these data suggest that sexually divergent activation of LC contributes to sex differences in parental behavior.

The activity patterns in LC-ACC neurons during retrieval closely resembled those from LC-wide recordings. This is consistent with our model that bursts of activity in LC during pup retrieval are pervasive. Pup retrieval evokes transient NA

(H) Scatterplot of coefficients (*r*) obtained by Spearman correlation of the duration of the retrieval events and the duration of intervals between retrieval events with the magnitude of LC-ACC responses during pup retrieval. Gray dots represent correlations that did not reach significance.

(I) Schematic of our viral strategy to express the GRAB[NE] sensor in ACC.

(J) Plots of mean fluorescent GRAB[NE] signal from ACC during pup retrieval events in dams (n = 6) and sires (n = 4). (Top) Heatmap wherein each row is the mean activity across all sessions from one mouse. (Bottom) Mean fluorescence trace for all mice. Data are aligned to pup contact.

(K) Plot comparing the AUC of fluorescent GRAB[NE] signal from ACC during pup retrieval events extending 2 s from pup contact with 2 s of baseline (paired t test, *p = 0.0173).

(L) Representative ΔF/F trace of GRAB[NE] fluorescence reflecting NA release while a dam interacted with pups. The black line above the trace indicates the time period when the dam was retrieving the pups to the nest.

(M) Schematic of the viral strategy used to express inhibitory DREADDs in LC-ACC neurons.

(N) Behavioral paradigm.

(O) Photomicrograph of a coronal brain section showing hM4D(Gi) expression in LC neurons that project to ACC (red) and TH antibody staining.

(P) Scatterplot of mean latency index (±SEM) in GFP-expressing dams (green) injected with saline or clozapine (n = 10) and hM4D(Gi)-expressing dams (orange) injected with saline or clozapine (n = 9). Ordinary one-way ANOVA, **p = 0.0075; Benjamini, Krieger, and Yekutieli test, clozapine, GFP vs. clozapine, hM4D(Gi) *p = 0.0137, saline, hM4D(Gi) vs. clozapine, hM4D(Gi) **p < 0.0028, saline, GFP vs. clozapine, hM4D(Gi) *p = 0.0072.

release in ACC, establishing a functional noradrenergic connection between LC and ACC during parental behavior. Indeed, when we selectively inactivated the LC-ACC, pup retrieval behavior was disrupted in early PPDs consistent with the results from inactivating all ACC^{CAMKII} (Figure 7). Based on our data as a whole, we conclude that ACC maintains sex-dependent sensitivity to pup distress in coordination with the noradrenergic system. We propose that parental behavior constitutes a tractable model to reveal the neural mechanisms by which social perception of distress can influence decisions.

Limitations of the study

There are several important caveats to be mindful of in interpreting our work. While our data strongly suggest that ACC modulation is necessary for accurate and timely parenting, we were not able to show that augmentation of ACC activity improved sires' retrieval performance. Chemogenetics lacks the temporal precision likely necessary to recapitulate the phasic activation of ACC, and optimal timing for optogenetic manipulations will be very difficult to achieve. Also, we monitored population activity of excitatory and inhibitory neurons in ACC during retrieval using photometry. Fiber photometry does not permit isolation of individual neurons. It will be important to assess the contribution of more specific cell types and individual neurons in ACC during parenting behaviors in future studies. The GRAB$_{NE}$ sensor we used to monitor NA release in ACC is not restricted to cells that express noradrenergic receptors endogenously and does not report the postsynaptic response. Therefore, sex-dependent sensitivity to NA in ACC remains to be tested. Future work is needed to identify the specific cell populations in ACC that receive noradrenergic input and the role of specific noradrenergic receptors in ACC during parenting. Using pharmacological manipulations of noradrenergic receptors can provide a mechanistic understanding of the role of NA in ACC during complex social behaviors.

STAR★METHODS

Detailed methods are provided in the online version of this paper and include the following:

- KEY RESOURCES TABLE
- RESOURCE AVAILABILITY
  - Lead contact
  - Materials availability
  - Data and code availability
- EXPERIMENTAL MODEL AND STUDY PARTICIPANT DETAILS
  - Animals
- METHOD DETAILS
  - Viruses
  - Histology
  - Pup retrieval assay
  - Pups in a jar experiment
  - Pup USVs recordings
  - Behavioral assay for brain-wide *c-fos* induction
  - Clearing protocol/*c-fos* staining

- Lightsheet imaging
- Stereotaxic injections
- Fiber photometry recordings and data analysis
- Chemogenetic inhibition
- QUANTIFICATION AND STATISTICAL ANALYSIS
  - Statistical analysis for *c-fos* mapping

REFERENCES

1. Kohl, J., Autry, A.E., and Dulac, C. (2017). The neurobiology of parenting: A neural circuit perspective. Bioessays *39*, 1–11. https://doi.org/10.1002/bies.201600159.

2. Dulac, C., O'Connell, L.A., and Wu, Z. (2014). Neural control of maternal and paternal behaviors. Science *345*, 765–770. https://doi.org/10.1126/science.1253291.

3. Lonstein, J.S., and De Vries, G.J. (2000). Sex differences in the parental behavior of rodents. Neurosci. Biobehav. Rev. *24*, 669–686. https://doi.org/10.1016/S0149-7634(00)00036-1.

4. Rogers, F.D., and Bales, K.L. (2019). Mothers, Fathers, and Others: Neural Substrates of Parental Care. Trends Neurosci. *42*, 552–562. https://doi.org/10.1016/j.tins.2019.05.008.

5. Numan, M. (2020). The Parental Brain Mechanisms, Development an Evolution (Oxford University Press).

6. Lukas, D., and Huchard, E. (2014). The evolution of infanticide by males in mammalian societies. Science *346*, 841–844. https://doi.org/10.1126/science.1257226.

7. Jeon, D., Kim, S., Chetana, M., Jo, D., Ruley, H.E., Lin, S.-Y., Rabah, D., Kinet, J.-P., and Shin, H.-S. (2010). Observational fear learning involves affective pain system and Cav1.2 Ca2+ channels in ACC. Nat. Neurosci. *13*, 482–488. https://doi.org/10.1038/nn.2504.

8. Burkett, J.P., Andari, E., Johnson, Z.V., Curry, D.C., de Waal, F.B.M., and Young, L.J. (2016). Oxytocin-dependent consolation behavior in rodents. Science *351*, 375–378. https://doi.org/10.1126/science.aac4785.

9. Li, L., Zhang, L.-Z., He, Z.-X., Ma, H., Zhang, Y.-T., Xun, Y.-F., Yuan, W., Hou, W.-J., Li, Y.-T., Lv, Z.-J., et al. (2021). Dorsal raphe nucleus to anterior cingulate cortex 5-HTergic neural circuit modulates consolation and sociability. Elife *10*, e67638. https://doi.org/10.7554/eLife.67638.

10. Smith, M.L., Asada, N., and Malenka, R.C. (2021). Anterior cingulate inputs to nucleus accumbens control the social transfer of pain and analgesia. Science *371*, 153–159. https://doi.org/10.1126/science.abe304.

11. Wu, Y.E., Dang, J., Kingsbury, L., Zhang, M., Sun, F., Hu, R.K., and Hong, W. (2021). Neural control of affiliative touch in prosocial interaction. Nature *599*, 262–267. https://doi.org/10.1038/s41586-021-03962-w.

12. Terranova, J.I., Yokose, J., Osanai, H., Marks, W.D., Yamamoto, J., Ogawa, S.K., and Kitamura, T. (2022). Hippocampal-amygdala memory circuits govern experience-dependent observational fear. Neuron *110*, 1416–1431.e13. https://doi.org/10.1016/j.neuron.2022.01.019.

13. Rudebeck, P.H., Walton, M.E., Smyth, A.N., Bannerman, D.M., and Rushworth, M.F.S. (2006). Separate neural pathways process different decision costs. Nat. Neurosci. *9*, 1161–1168. https://doi.org/10.1038/nn1756.

14. Guo, B., Chen, J., Chen, Q., Ren, K., Feng, D., Mao, H., Yao, H., Yang, J., Liu, H., Liu, Y., et al. (2019). Anterior cingulate cortex dysfunction underlies social deficits in Shank3 mutant mice. Nat. Neurosci. *22*, 1223–1234. https://doi.org/10.1038/s41593-019-0445-9.

15. Slotnick, B.M. (1967). Disturbances of maternal behavior in the rat following lesions of the cingulate cortex. Behaviour *29*, 204–236. https://doi.org/10.1163/156853967x00127.

16. Li, T., Horta, M., Mascaro, J.S., Bijanki, K., Arnal, L.H., Adams, M., Barr, R.G., and Rilling, J.K. (2018). Explaining individual variation in paternal brain responses to infant cries. Physiol. Behav. *193*, 43–54. https://doi.org/10.1016/j.physbeh.2017.12.033.

17. Berridge, C.W., and Waterhouse, B.D. (2003). The locus coeruleus–noradrenergic system: modulation of behavioral state and state-dependent cognitive processes. Brain Res. Rev. *42*, 33–84. https://doi.org/10.1016/S0165-0173(03)00143-7.

18. McCall, J.G., Al-Hasani, R., Siuda, E.R., Hong, D.Y., Norris, A.J., Ford, C.P., and Bruchas, M.R. (2015). CRH Engagement of the Locus Coeruleus Noradrenergic System Mediates Stress-Induced Anxiety. Neuron *87*, 605–620. https://doi.org/10.1016/j.neuron.2015.07.002.

19. Thomas, S.A., and Palmiter, R.D. (1997). Impaired Maternal Behavior in Mice Lacking Norepinephrine and Epinephrine. Cell *91*, 583–592. https://doi.org/10.1016/S0092-8674(00)80446-8.

20. Sewell, G.D. (1970). Ultrasonic Communication in Rodents. Nature *227*, 410. https://doi.org/10.1038/227410a0.

21. Noirot, E. (1972). Ultrasounds and maternal behavior in small rodents. Dev. Psychobiol. *5*, 371–387. https://doi.org/10.1002/dev.420050410.

22. Ehret, G., and Bernecker, C. (1986). Low-frequency sound communication by mouse pups (Mus musculus): wriggling calls release maternal behaviour. Anim. Behav. *34*, 821–830. https://doi.org/10.1016/S0003-3472(86)80067-7.

23. Ehret, G. (1987). Left hemisphere advantage in the mouse brain for recognizing ultrasonic communication calls. Nature *325*, 249–251. https://doi.org/10.1038/325249a0.

24. Ehret, G. (2005). Infant Rodent Ultrasounds ? A Gate to the Understanding of Sound Communication. Behav. Genet. *35*, 19–29. https://doi.org/10.1007/s10519-004-0853-8.

25. Liu, R.C., Miller, K.D., Merzenich, M.M., and Schreiner, C.E. (2003). Acoustic variability and distinguishability among mouse ultrasound vocalizations. J. Acoust. Soc. Am. *114*, 3412–3422. https://doi.org/10.1121/1.1623787.

26. Dvorkin, R., and Shea, S.D. (2022). Precise and pervasive phasic bursting in locus coeruleus during maternal behavior in mice. J. Neurosci. *42*, 2986–2999. https://doi.org/10.1523/JNEUROSCI.0938-21.2022.

27. Schwarz, L.A., Miyamichi, K., Gao, X.J., Beier, K.T., Weissbourd, B., DeLoach, K.E., Ren, J., Ibanes, S., Malenka, R.C., Kremer, E.J., and Luo, L. (2015). Viral-genetic tracing of the input–output organization of a central noradrenaline circuit. Nature *524*, 88–92. https://doi.org/10.1038/nature14600.

28. Kebschull, J.M., Garcia da Silva, P., Reid, A.P., Peikon, I.D., Albeanu, D.F., and Zador, A.M. (2016). High-Throughput Mapping of Single-Neuron Projections by Sequencing of Barcoded RNA. Neuron *91*, 975–987. https://doi.org/10.1016/j.neuron.2016.07.036.

29. Fillinger, C., Yalcin, I., Barrot, M., and Veinante, P. (2017). Afferents to anterior cingulate areas 24a and 24b and midcingulate areas 24a′ and 24b′ in the mouse. Brain Struct. Funct. *222*, 1509–1532. https://doi.org/10.1007/s00429-016-1290-1.

30. Joshi, S., and Gold, J.I. (2022). Context-dependent relationships between locus coeruleus firing patterns and coordinated neural activity in the anterior cingulate cortex. Elife *11*, e63490. https://doi.org/10.7554/eLife.63490.

31. Liu, H.-X., Lopatina, O., Higashida, C., Fujimoto, H., Akther, S., Inzhutova, A., Liang, M., Zhong, J., Tsuji, T., Yoshihara, T., et al. (2013). Displays of paternal mouse pup retrieval following communicative interaction with maternal mates. Nat. Commun. *4*, 1346. https://doi.org/10.1038/ncomms2336.

32. Wu, Z., Autry, A.E., Bergan, J.F., Watabe-Uchida, M., and Dulac, C.G. (2014). Galanin neurons in the medial preoptic area govern parental behaviour. Nature *509*, 325–330. https://doi.org/10.1038/nature13307.

33. Kohl, J., Babayan, B.M., Rubinstein, N.D., Autry, A.E., Marin-Rodriguez, B., Kapoor, V., Miyamishi, K., Zweifel, L.S., Luo, L., Uchida, N., et al. (2018). Functional circuit architecture underlying parental behaviour. Nature *556*, 326–331. https://doi.org/10.1038/s41586-018-0027-0.

34. Stagkourakis, S., Smiley, K.O., Williams, P., Kakadellis, S., Ziegler, K., Bakker, J., Brown, R.S.E., Harkany, T., Grattan, D.R., and Broberger, C. (2020). A Neuro-hormonal Circuit for Paternal Behavior Controlled by a Hypothalamic Network Oscillation. Cell *182*, 960–975.e15. https://doi.org/10.1016/j.cell.2020.07.007.

35. Krishnan, K., Lau, B.Y.B., Ewall, G., Huang, Z.J., and Shea, S.D. (2017). MECP2 regulates cortical plasticity underlying a learned behaviour in adult female mice. Nat. Commun. *8*, 14077. https://doi.org/10.1038/ncomms14077.

36. Renier, N., Adams, E.L., Kirst, C., Wu, Z., Azevedo, R., Kohl, J., Autry, A.E., Kadiri, L., Umadevi Venkataraju, K., Zhou, Y., et al. (2016). Mapping of Brain Activity by Automated Volume Analysis of Immediate Early Genes. Cell *165*, 1789–1802. https://doi.org/10.1016/j.cell.2016.05.007.

37. Pfaff, D., and Keiner, M. (1973). Atlas of estradiol-concentrating cells in the central nervous system of the female rat. J. Comp. Neurol. *151*, 121–158. https://doi.org/10.1002/cne.901510204.

38. Freund-Mercier, M.J., Stoeckel, M.E., Palacios, J.M., Pazos, A., Reichhart, J.M., Porte, A., and Richard, P. (1987). Pharmacological characteristics and anatomical distribution of [3H]oxytocin-binding sites in the Wistar rat brain studied by autoradiography. Neuroscience *20*, 599–614. https://doi.org/10.1016/0306-4522(87)90113-8.

39. Numan, M., and Numan, M. (1996). A lesion and neuroanatomical tract-tracing analysis of the role of the bed nucleus of the stria terminalis in retrieval behavior and other aspects of maternal responsiveness in rats. Dev. Psychobiol. *29*, 23–51. https://doi.org/10.1002/(SICI)1098-2302(199601)29:1<23::AID-DEV2>3.0.CO;2-O.

40. Bakowska, J.C., and Morrell, J.I. (1997). Atlas of the neurons that express mRNA for the long form of the prolactin receptor in the forebrain of the female rat. J. Comp. Neurol. *386*, 161–177. https://doi.org/10.1002/(SICI)1096-9861(19970922)386:2<161::AID-CNE1>3.0.CO;2-#.

41. Matsushita, N., Muroi, Y., Kinoshita, K.i., and Ishii, T. (2015). Comparison of c-Fos expression in brain regions involved in maternal behavior of virgin and lactating female mice. Neurosci. Lett. *590*, 166–171. https://doi.org/10.1016/j.neulet.2015.02.003.

42. Numan, M., Rosenblatt, J.S., and Komisaruk, B.R. (1977). Medial preoptic area and onset of maternal behavior in the rat. J. Comp. Physiol. Psychol. *91*, 146–164. https://doi.org/10.1037/h0077304.

43. Numan, M., and Numan, M.J. (1994). Expression of Fos-Like Immunoreactivity in the Preoptic Area of Maternally Behaving Virgin and Postpartum Rats. Behav. Neurosci. *108*, 379–394. https://doi.org/10.1037/0735-7044.108.2.379.

44. Pedersen, C.A., Caldwell, J.D., Walker, C., Ayers, G., and Mason, G.A. (1994). Oxytocin Activates the Postpartum Onset of Rat Maternal Behavior in the Ventral Tegmental and Medial Preoptic Areas. Behav. Neurosci. *108*, 1163–1171. https://doi.org/10.1037/0735-7044.108.6.1163.

45. Lee, A., Clancy, S., and Fleming, A.S. (1999). Mother rats bar-press for pups: effects of lesions of the mpoa and limbic sites on maternal behavior and operant responding for pup-reinforcement. Behav. Brain Res. *100*, 15–31. https://doi.org/10.1016/S0166-4328(98)00109-0.

46. Kuroda, K.O., Meaney, M.J., Uetani, N., Fortin, Y., Ponton, A., and Kato, T. (2007). ERK-FosB signaling in dorsal MPOA neurons plays a major role in the initiation of parental behavior in mice. Mol. Cell. Neurosci. *36*, 121–131. https://doi.org/10.1016/j.mcn.2007.05.010.

47. Kelly, A.M., Ong, J.Y., Witmer, R.A., and Ophir, A.G. (2020). Paternal deprivation impairs social behavior putatively via epigenetic modification to lateral septum vasopressin receptor. Sci. Adv. *6*, eabb9116. https://doi.org/10.1126/sciadv.abb9116.

48. Numan, M., Bress, J.A., Ranker, L.R., Gary, A.J., DeNicola, A.L., Bettis, J.K., and Knapp, S.E. (2010). The importance of the basolateral/basomedial amygdala for goal-directed maternal responses in postpartum rats. Behav. Brain Res. *214*, 368–376. https://doi.org/10.1016/j.bbr.2010.06.006.

49. Okabe, S., Nagasawa, M., Kihara, T., Kato, M., Harada, T., Koshida, N., Mogi, K., and Kikusui, T. (2013). Pup odor and ultrasonic vocalizations synergistically stimulate maternal attention in mice. Behav. Neurosci. *127*, 432–438. https://doi.org/10.1037/a0032395.

50. Rickenbacher, E., Perry, R.E., Sullivan, R.M., and Moita, M.A. (2017). Freezing suppression by oxytocin in central amygdala allows alternate defensive behaviours and mother-pup interactions. Elife *6*, e24080. https://doi.org/10.7554/eLife.24080.

51. Nawaratne, V., Leach, K., Suratman, N., Loiacono, R.E., Felder, C.C., Armbruster, B.N., Roth, B.L., Sexton, P.M., and Christopoulos, A. (2008). New Insights into the Function of M$_4$ Muscarinic Acetylcholine Receptors Gained Using a Novel Allosteric Modulator and a DREADD (Designer Receptor Exclusively Activated by a Designer Drug). Mol. Pharmacol. *74*, 1119–1131. https://doi.org/10.1124/mol.108.049353.

52. Gomez, J.L., Bonaventura, J., Lesniak, W., Mathews, W.B., Sysa-Shah, P., Rodriguez, L.A., Ellis, R.J., Richie, C.T., Harvey, B.K., Dannals, R.F., et al. (2017). Chemogenetics revealed: DREADD occupancy and activation via converted clozapine. Science *357*, 503–507. https://doi.org/10.1126/science.aan2475.

53. Fillinger, C., Yalcin, I., Barrot, M., and Veinante, P. (2018). Efferents of anterior cingulate areas 24a and 24b and midcingulate areas 24a' and 24b' in the mouse. Brain Struct. Funct. *223*, 1747–1778. https://doi.org/10.1007/s00429-017-1585-x.

54. Koga, K., Yamada, A., Song, Q., Li, X.-H., Chen, Q.-Y., Liu, R.-H., Ge, J., Zhan, C., Furue, H., Zhuo, M., et al. (2020). Ascending noradrenergic excitation from the locus coeruleus to the anterior cingulate cortex. Mol. Brain *13*, 49. https://doi.org/10.1186/s13041-020-00586-5.

55. Feng, J., Zhang, C., Lischinsky, J.E., Jing, M., Zhou, J., Wang, H., Zhang, Y., Dong, A., Wu, Z., Wu, H., et al. (2019). A Genetically Encoded Fluorescent Sensor for Rapid and Specific In Vivo Detection of Norepinephrine. Neuron *102*, 745–761.e8. https://doi.org/10.1016/j.neuron.2019.02.037.

56. Inada, K., Hagihara, M., Tsujimoto, K., Abe, T., Konno, A., Hirai, H., Kiyonari, H., and Miyamichi, K. (2022). Plasticity of neural connections underlying oxytocin-mediated parental behaviors of male mice. Neuron *110*, 2009–2023.e5. https://doi.org/10.1016/j.neuron.2022.03.033.

57. Isaacson, J.S., and Scanziani, M. (2011). How Inhibition Shapes Cortical Activity. Neuron *72*, 231–243. https://doi.org/10.1016/j.neuron.2011.09.027.

58. Poe, G.R., Foote, S., Eschenko, O., Johansen, J.P., Bouret, S., Aston-Jones, G., Harley, C.W., Manahan-Vaughan, D., Weinshenker, D., Valentino, R., et al. (2020). Locus coeruleus: a new look at the blue spot. Nat. Rev. Neurosci. *21*, 644–659. https://doi.org/10.1038/s41583-020-0360-9.

59. Ross, J.A., and Van Bockstaele, E.J. (2020). The Locus Coeruleus- Norepinephrine System in Stress and Arousal: Unraveling Historical, Current, and Future Perspectives. Front. Psychiatry *11*, 601519. https://doi.org/10.3389/fpsyt.2020.601519.

60. Curtis, A.L., Bethea, T., and Valentino, R.J. (2006). Sexually Dimorphic Responses of the Brain Norepinephrine System to Stress and Corticotropin-Releasing Factor. Neuropsychopharmacology *31*, 544–554. https://doi.org/10.1038/sj.npp.1300875.

61. Dana, H., Sun, Y., Mohar, B., Hulse, B.K., Kerlin, A.M., Hasseman, J.P., Tsegaye, G., Tsang, A., Wong, A., Patel, R., et al. (2019). High-performance calcium sensors for imaging activity in neuronal populations and microcompartments. Nat. Methods *16*, 649–657. https://doi.org/10.1038/s41592-019-0435-6.

62. Krashes, M.J., Koda, S., Ye, C., Rogan, S.C., Adams, A.C., Cusher, D.S., Maratos-Flier, E., Roth, B.L., and Lowell, B.B. (2011). Rapid, reversible activation of AgRP neurons drives feeding behavior in mice. J. Clin. Invest. *121*, 1424–1428. https://doi.org/10.1172/JCI46229.

63. Xie, Y., Huang, L., Corona, A., Pagliaro, A.H., and Shea, S.D. (2023). A dopaminergic reward prediction error signal shapes maternal behavior in mice. Neuron *111*, 557–570.e7. https://doi.org/10.1016/j.neuron.2022.11.019.

64. Friard, O., and Gamba, M. (2016). BORIS: a free, versatile open-source event-logging software for video/audio coding and live observations. Methods Ecol. Evol. *7*, 1325–1330. https://doi.org/10.1111/2041-210X.12584.

65. Venables, W.N., and Ripley, B.D. (2002). MASS: Modern Applied Statistics with S (Springer).

66. O'Hara, R.B., and Kotze, D.J. (2010). Do not log-transform count data: *Do not log-transform count data*. Methods Ecol. Evol. *1*, 118–122. https://doi.org/10.1111/j.2041-210X.2010.00021.x.

67. Benjamini, Y., and Hochberg, Y. (1995). Controlling the False Discovery Rate: A Practical and Powerful Approach to Multiple Testing. J. R. Stat. Soc. Ser. B Methodol. *57*, 289–300. https://doi.org/10.1111/j.2517-6161.1995.tb02031.x.

STAR★METHODS

KEY RESOURCES TABLE

REAGENT or RESOURCE	SOURCE	IDENTIFIER
Antibodies		
Chicken anti-TH	Abcam	Cat #76442; RRID: AB_1524535
Rabbit anti-GFP	Invitrogen	Cat# A6455; RRID: AB_221570
Goat anti-chicken Alexa Fluor 594	Invitrogen	Cat# A11042; RRID: AB_2534099
Goat anti-chicken Alexa Fluor 488	Invitrogen	Cat# A11039; RRID: AB_2534096
Goat anti-rabbit Alexa Fluor 488	Invitrogen	Cat# A11008; RRID: AB_143165
Bacterial and virus strains		
pGP-AAV-syn-FLEX-jGCaMP7s-WPRE (AAV9)	(Dana et al.)[61]	Addgene_104491
pAAV-CaMKIIa-EGFP (AAV8)	Bryan Roth	Addgene_50469
pAAV-CaMKIIa-hM4D(Gi)-mCherry (AAV8)	Bryan Roth	Addgene_50477
AAV.CamKII.GCaMP6s.WPRE.SV40 (AAV9)	James M. Wilson	Addgene_107790
pAAV-CAG-tdTomato	Edward Boyden	Addgene_59462
pENN.AAV.hSyn.Cre.WPRE.hGH	James M. Wilson	Addgene_105553
pAAV.synP.DIO.EGFP.WPRE.hGH (AAV9)	Ian Wickersham	Addgene_100043
pAAV-hSyn-DIO-hM4D(Gi)-mCherry (AAV5)	(Krashes et al.)[62]	Addgene_44362
AAV9-hSyn-NE2h	(Feng at al)[55]	Vigene Biosciences_YL10074-AAV9
Chemicals, peptides, and recombinant proteins		
DirectPCR	Viagen	Cat# 402-E RRID: N/A
Proteinase K	Invitrogen	Cat# AM2548 RRID: N/A
Euthasol	Virbac	Cat# 200-071 RRID: N/A
4% paraformaldehyde	FD Neurotechnologies	Cat# PF101 RRID: N/A
OCT compound	Sakura	Cat# 4583 RRID: N/A
Normal goat serum	Vector Laboratories	Cat# S-1000-20 RRID: N/A
Triton X-100	Sigma	Cat# T8787 RRID: N/A
Meloxicam	Metacam	Cat# NDC 0010-6013-01 RRID: N/A
Ketamine	Ketaset	Cat# NDC 54771-2013 RRID: N/A
Xylazine	AnaSed	Cat# NDC 59399-110-20 RRID: N/A
Vectashield	Vector Laboratories	Cat# H-1200-10 RRID: N/A
Vetbond	Amazon	Cat# B079QJXK46 RRID: N/A
Isofluorine	Covetrus	Cat# 029405 RRID: N/A
Clozapine dihydrochloride (water soluble)	Hello Bio	Cat # HB6129 RRID: N/A

Continued

REAGENT or RESOURCE	SOURCE	IDENTIFIER
Critical commercial assays		
GoTaq Green Master Mix	Promega	M7123 RRID: N/A
Experimental models: Organisms/strains		
CBA/CaJ	The Jackson Laboratory	RRID:IMSR_JAX:000654
DBH-CRE	MMRRC	RRID:MMRRC_032081-UCD
VGAT-CRE	The Jackson Laboratory	RRID:IMSR_JAX:016962
Software and algorithms		
Zen	Zeiss	https://www.zeiss.com/microscopy/en/products/software/zeiss-zen.html
MATLAB R2019b	MathWorks	https://www.mathworks.com/products/matlab.html
Adobe Illustrator	Adobe	https://www.adobe.com/products/illustrator
Prism	GraphPad by Dotmatics	https://www.graphpad.com
Custom analysis code	Zenodo	https://doi.org/10.5281/zenodo.7998686
Other		
Microtome	Leica	SM 2010R RRID: N/A
4oz. glass jars	AOZITA	B07VHBX3ZC RRID: N/A
Light-sheet microscope (Ultramicroscope II)	LaVision Biotec	N/A
Confocal microscope	Zeiss	LSM 710 RRID: N/A
Optic fibers for fiber photometry	Newdoon	http://www.newdoon.com/index.php?route=product/product&product_id=271 RRID: N/A
Patch cord for fiber photometry	Doric Lenses	Cat# P99414-01 RRID: N/A
LED driver	Thorlabs	Cat# LEDD1B RRID: N/A
Rotary joint for fiber photometry	Doric Lenses	Cat# FRJ_FC_FC RRID: N/A
Photoreceivers	Newport	Cat# 2151 RRID: N/A
USV Microphone (CM16/CMPA-5V)	Avisoft-Bioacoustics	Cat # 40013 RRID: N/A
470nm and 565nm LED light sources	Thorlabs	Cat# M470F3 and M565F3 RRID: N/A

RESOURCE AVAILABILITY

Lead contact
Further information and requests for resources and reagents should be directed to and will be fulfilled by the lead contact, Stephen D. Shea (sshea@cshl.edu).

Materials availability
This study did not generate new unique reagents.

Data and code availability
- All data reported in this paper will be shared by the lead contact upon request.
- All original MATLAB analysis code has been deposited at Zenodo and made publicly available as of the date of acceptance for publication. DOIs are listed in the key resources table.
- Any additional information required to reanalyze the data reported in this paper is available from the lead contact upon request.

EXPERIMENTAL MODEL AND STUDY PARTICIPANT DETAILS

Animals

Adult mice (8–14 weeks old) were maintained on a 12h/12 h light-dark cycle (lights on 07:00h) and received food and water ad libitum. Genotypes used were CBA/CaJ (The Jackson Laboratory, #000654), VGAT-Cre (Slc32a1tm2(cre)Lowl/J, The Jackson Laboratory, #016962), and DBH-Cre (Tg(Dbh-cre)KH212Gsat/Mmucd, unfrozen stock, MMRRC). All mice used for pup retrieval experiments were primiparous except for the second pregnancy experiment on Figure S3. All procedures were conducted in accordance with the National Institutes of Health's Guide for the care and use of laboratory animals and approved by the Cold Spring Harbor Laboratory Institutional Animal Care and Use Committee.

METHOD DETAILS

Viruses

We used the following commercially available viruses: pGP-AAV-syn-FLEX-jGCaMP7s-WPRE (3.1×10^{13} GC/mL, Addgene, 104491-AAV9); pAAV-CaMKIIa-EGFP (2.1×10^{13} GC/mL, Addgene, 50469-AAV8); pAAV-CaMKIIa-hM4D(Gi)-mCherry (2.1×10^{13} GC/mL, Addgene, 50477-AAV8); AAV.CamKII.GCaMP6s.WPRE.SV40 (2.1×10^{13} GC/mL, Addgene, 107790-AAV9); pAAV-CAG-tdTomato (1.3×10^{13} GC/mL, Addgene, 59462-AAVrg); AAV9-hSyn-NE2h (2.37×10^{13} GC/mL, Vigene Biosciences, YL10074-AAV9); pENN.AAV.hSyn.Cre.WPRE.hGH (1.2×10^{13} GC/mL, Addgene, 105553-AAVrg); pAAV.synP.DIO.EGFP.WPRE.hGH (4.3×10^{13} GC/mL, Addgene, 100043-AAV9); pAAV-hSyn-DIO-hM4D(Gi)-mCherry (1.2×10^{13} GC/mL, Addgene, 44362-AAV5).

Histology

We used the protocol from Xie et al.,[63] animals were deeply anesthetized with a lethal dose of Euthasol (Virbac, 200-071) via intraperitoneal injection, and were subsequently transcardially perfused with phosphate-buffered saline (1X PBS) and 4% paraformaldehyde (PFA; FD Neurotechnologies, PF101) at a flow rate of 7.5 mL/min. Brains were post-fixed in 4% PFA overnight at 4 Celsius and then transferred to a 30% sucrose solution in PBS. Brains were embedded with OCT compound (Sakura, 4583) and sectioned frozen at 50 μm on a sliding microtome (Leica, SM 2010R). For immunostaining, free-floating sections were washed with PBS 3 times and blocked in 5% normal goat serum (NGS, Vector Laboratories, S-1000-20) and 0.1% Triton X-100 (Sigma, T8787) at room temperature (RT) for 1.5 h. Sections were incubated overnight with primary antibodies in a solution containing 0.5% NGS and 0.1% Triton X-100 at 4 Celsius. The next day, sections were incubated for 2 h with secondary antibodies in a solution containing 0.5% NGS and 0.1% Triton X-100 at room temperature. After washing 3 times with 1X PBS, sections were mounted on coverslips with Fluoromount-G (SouthernBiotech, 0100-01). Primary antibodies including chicken anti-TH antibody (Abcam, 76442) and rabbit anti-GFP antibody (Invitrogen, A6455) were used. Secondary antibodies including Alexa Fluor 594 goat anti-chicken (Invitrogen, A11042), Alexa Fluor 488 goat anti-chicken (Invitrogen, A11039) and Alexa Fluor 488 goat anti-rabbit (Invitrogen, A11008) were used.

Pup retrieval assay

Briefly, (1) The test subject was habituated with 5 pups in the nest of the home cage for 5 min in a soundproof behavioral box, (2) the pups were removed from the cage for 2 min, and (3) then the pups were scattered in the cage. The first pup was placed in the nest and then moving clockwise, a pup was placed in each corner and one in the center. Each test subject had a maximum of 5 min to gather the pups to the nest. The same procedure was repeated on PPD0-PPD5. All assays were performed in the dark during the light cycle and videos were recorded for further analysis.

For the behavioral analysis, we calculated the latency index for each mouse to gather all pups using the formula:

$$latency\ index = [(t1 - t0) + (t2 - t0) + \cdots + (tn - t0)]/(n \times L)$$

where: n = # of pups outside the nest, t0 = start of trial, tn = time of nth pup gathered, L = trial length.

The same experiment was conducted in a clean/novel cage with different mice.

We quantified the duration of each retrieval event measured from the time the subject made pup contact to the time it drops the nest in the nest in the home cage. We also quantified the duration of intervals between retrieval events measured from the end of the previous retrieval event to the start of the next one in the home cage.

Pups in a jar experiment

All pups from the litter were placed in a 4oz. glass jar with a plastic lid with holes in it (AOZITA; B07VHBX3ZC). The test subjects were able to hear and smell the pups in the jar, but were not able to touch them. The animal's behavior was recorded for 5 min with the pups in the jar and 5 min with an empty jar in the home cage. Interactions with the lid of the jar were quantified as a proxy of motivation for the test subject to interact with the pups. All behaviors were scored with the software BORIS.[64] An interaction with the jar was quantified when the test subject was in close proximity to the lid of the jar and facing it, either touching, biting, or sniffing it.

Pup USVs recordings

To confirm the jar was enough to put the pups in distress, we recorded USVs for 5 min when the pups were in the nest in the home cage and 5 min with the pups in a jar. All pups used to record USVs were 0–5 days old. We placed the pups in a jar and placed the jar in the home cage. We started recording the vocalizations using a USV microphone (Condenser ultrasound microphone Avisoft-Bioacoustics CM16/CMPA-5V; part # 40013) 1 min after placing the pups in the jar. To record the vocalizations in the nest, we removed the parents from the home cage. We started recording USVs 1 min after removing the parents.

Behavioral assay for brain-wide *c-fos* induction

Male and female wild-type CBA/CaJ mice breeding pairs were made at 8-10 weeks-old. The experiment included four behavioral groups, and it was performed on PPD3. Baseline: the test subject was kept in the home cage with the pups in the nest for a 3-h period. Isolated: the test subject was kept in the home cage without the pups for a 3-h period. Reunion: the test subject was kept in the home cage without the pups for a 90-min period, and then all pups were returned in the nest for a second 90-min period. Retrieval: the test subject was kept in the home cage without the pups for 90 min, and then all pups were returned scattered in the cage for 90 min. The experiment was performed in dams and sires 12–14 weeks old. All experiments were performed in the dark during the light cycle in a soundproof behavioral box. All mice were perfused immediately after the experiment was done through the ascending aorta with 1% PBS, followed by 4% paraformaldehyde (PFA) in 0.1 M PBS (pH 7.4). The brains were removed and post-fixed in paraformaldehyde overnight before starting the clearing protocol.

Clearing protocol/*c-fos* staining

All brains were cleared using the iDisco+ protocol.[36] Briefly, the fixed samples were washed in PBS and treated with a serial dilution of methanol, permeabilized with a solution containing dimethyl sulfoxide, blocked in donkey serum, and passively immunolabeled for *c-Fos* at 37 Celcius for 7 days (9F6 rabbit mAb 2200, Cell Signaling Technology) and Alexa Fluorophore 647 secondary antibodies at 37 Celcius for 7 days. Then, the samples were cleared with a combination of methanol and dichloromethane.[36]

Lightsheet imaging

Cleared samples were imaged in sagittal orientation (left hemisphere) on a light-sheet fluorescence microscope (Ultramicroscope II, LaVision Biotec) equipped with a sCMOS camera (Andor *Neo*) and a 4x/0.5 objective lens (MVPLAPO 4×) equipped with a 6-mm working distance dipping cap. Version v144 of the Imspector Microscope controller software was used. The samples were scanned with a step-size of 3 μm using the continuous light-sheet scanning method with the included contrast blending algorithm for the 640 nm and 595 nm channels (20 acquisitions per plane), and without horizontal scanning for the 480-nm channel.

Stereotaxic injections

All surgery was performed under aseptic conditions and body temperature was maintained with a heating pad. Standard surgical procedures were used for stereotaxic injection and implantation. Briefly, mice were anesthetized with isoflurane (2% in a mixture with oxygen, applied at 1.0 L/min), and head-fixed in a stereotaxic injection frame. Ketamine was used as an anesthetic.

To prepare mice for the photometry experiments, we first made a small craniotomy in each mouse, unilaterally. We then lowered a glass micropipette (tip diameter, ~20 μm) containing viral solution to reach the ACC (coordinates: +0.55 mm posterior to bregma, 0.3 mm lateral from midline, and −0.9 mm ventral from brain surface). For CAMKII photometry recordings, we used 0.2–0.3 μL of AAV.CamKII.GCaMP6s.WPRE.SV40 (AAV9); titer: 2.1×10^{13} GC/mL. For VGAT recordings, we used 0.2–0.3 μL of pGP-AAV-syn-FLEX-jGCaMP7s-WPRE (AAV9) injected into VGAT-cre mice; titer: 3.1×10^{13} GC/mL. The injection coordinates for the LC experiments were (+1.5mm posterior to lambda, 0.8mm lateral from the midline, and 2.8mm ventral from the brain surface). 0.4–0.6 μL of pGP-AAV-syn-FLEX-jGCaMP7s-WPRE (AAV9) were injected into DBH-cre mice; titer: 3.1×10^{13} GC/mL.

Viral solutions were delivered with pressure applications (5–20 psi, 5–20 ms at 1 Hz) controlled by a Picrospritzer and a pulse generator. The rate of injection was ~50 nL/min. The pipette was left in place for 5–10 min following the injection, and then slowly withdrawn. We then implanted optic fibers above injection locations in the mice dedicated for photometry experiments (coordinates: +0.55 mm anterior to bregma, 0.3 mm lateral from midline, and 0.9 mm vertical from brain surface). A head-bar was also mounted for head-restraint. We waited one week for the mice to recover from surgery and pair them with a mate. We then waited for the pups to be born to start recording the photometry signals.

For ACC chemogenetic experiments, infection of ACC was performed in both hemispheres. 0.2 μL of pAAV-CaMKIIa-hM4D(Gi)-mCherry (AAV8); titer: 2.1×10^{13} GC/mL was delivered to each hemisphere (coordinates: +0.55 mm posterior to bregma, ±0.3 mm lateral from midline, and −0.9 mm ventral from brain surface). For LC-ACC projection inhibition experiment, we injected 0.2 μL of a retrograde AAV.hsyn.CRE.WPRE; titer: 1.2×10^{13} GC/mL in ACC of female CBA/CaJ mice bilaterally, and 0.2–0.3 μL of pAAV-hSyn-DIO-hM4D(Gi)-mCherry (AAV5); titer: 1.2×10^{13} GC/mL bilaterally into the LC.

Fiber photometry recordings and data analysis

To record the activity of CamkII+ cells in ACC *in vivo*, we used a custom-made fiber photometry system to measure GCaMP6s signals in these neurons through an optical fiber (Fiber core diameter, 200 μm; Fiber length, 2.0 mm; NA, 0.37; Inper, Hangzhou, China) unilaterally implanted in ACC of 8–10 weeks-old male and female mice. Animals were habituated to the behavioral box in their home cage

for 10 min starting at least 1 day before parturition. 4 retrieval sessions were recorded each day were all pups from the litter were scattered in the cage, and the test subject was allowed to retrieve all the pups. Each session was 5 min long and sessions were separated by 2 min. For the second pregnancy experiment on Figure S5, we repeated the same procedure with the second litter of pups. The same behavioral procedures were used to record neural activity from all of the populations described below. GCaMP signals were detected and measured as follows: briefly, activity-dependent GCaMP was delivered by AAV to CamkII+ neurons under the expression of the CamkII promoter. An optical fiber cable was mated to the fiber implant in the ACC neurons before each optical recording session, and it was used to deliver 470 nm and 565 nm excitation light to the brain. The intensity of the light for excitation was adjusted to ~5–10 μW at the tip of the patch cord. The two wavelengths were sinusoidally modulated at 211 Hz and 180° out of phase. Green and red emitted light signals were filtered and split to separate photodetectors and digitally sampled at 6100 Hz via a data acquisition board (National Instruments, Model # NI USB-6211). Peaks were extracted by custom MATLAB software with an effective sampling rate of 211 Hz. Each signal was corrected for photobleaching by fitting the decay with a double exponential, and then normalized to a Z score. After subtracting the activity-independent red signal to correct for movement artifacts, the green signal was transformed back to absolute fluorescence and DF/F was computed relative to the mean of the measured fluorescence minus the mean of the baseline fluorescence. The resulting traces from each recording session were converted to a Z score to compare between subjects and across days. All data analysis was performed using custom written code in MATLAB.

To record activity of DBH+ cells in LC *in vivo*, we injected a cre-dependent AAV GCaMP7s into the LC of DBH-Cre mice and implanted a fiber unilaterally in the LC (Fiber core diameter, 200 μm; Fiber length, 5.5 mm; NA, 0.37; Inper, Hangzhou, China). The intensity of the light for excitation was adjusted to ~30 μW at the tip of the patch cord. To record the activity of inhibitory neurons in the ACC during parental behavior, we injected a cre-dependent AAV GCaMP7s into ACC of VGAT-Cre mice and implanted a fiber unilaterally in ACC (Fiber core diameter, 200 μm; Fiber length, 2.0 mm; NA, 0.37; Inper, Hangzhou, China). The intensity of the light for excitation was adjusted to ~5–10 μW at the tip of the patch cord. To record noradrenaline release in ACC, we used fiber photometry and a noradrenaline sensor. We injected AAV-hsyn-NE2h; titer: 2.37×10^{13} GC/mL into the cingulate cortex of CBA/CaJ mice and implanted a fiber unilaterally in the ACC (Fiber core diameter, 200 μm; Fiber length, 2.0 mm; NA, 0.37; Inper, Hangzhou, China). The intensity of the light for excitation was adjusted to ~5–10 μW at the tip of the patch cord.

To record the activity of LC-ACC neurons *in vivo,* we injected 0.2 μL of a retrograde AAV.hsyn.CRE.WPRE; titer: 1.2×10^{13} GC/mL in ACC of female CBA/CaJ mice, and 0.2–0.3 μL of pGP-AAV-syn-FLEX-jGCaMP7s-WPRE (AAV9); titer: 3.1×10^{13} GC/mL into the LC and implanted a fiber unilaterally in LC (Fiber core diameter, 200 μm; Fiber length, 5.5 mm; NA, 0.37; Inper, Hangzhou, China). The intensity of the light for excitation was adjusted to ~30 μW at the tip of the patch cord.

For pup retrieval photometry experiments, we recorded 4 retrieval sessions each day. All pups from the litter were scattered in the cage, and the test subject was allowed to retrieve all the pups. Each session was 5 min long and sessions were separated by 2 min.

Chemogenetic inhibition

Mice were habituated to the behavioral box for 10 min at least 24h before the experiment. Mice were maintained on a 12h/12 h light-dark cycle (lights on 10:00 h) and received food and water ad libitum. During the dark phase, test subjects were habituated in their home cage for 10 min. CBA/CaJ mice expressing hM4D(Gi) were injected intraperitoneally (i.p.) with either saline (0.9% NaCl) or clozapine (0.1 mg/kg) (HelloBio, Inc.) dissolved in saline. The injection of clozapine or saline was alternating in each mouse every other day; P0 and P2 clozapine and P1 and P3 saline. Twenty minutes after the injections, all pups were scattered in the home cage and the test subject's behavior was recorded for 10 min. Then, all pups were placed in a jar for 5 min and videos were recorded. Lastly, the test subjects were exposed to an empty jar and videos were recorded. All videos were manually scored using BORIS.[64]

For the LC-ACC neuron selective inactivation experiments, we bilaterally injected a retrograde AAV.hsyn.CRE.WPRE (1.2×10^{13} GC/mL) in ACC of female CBA/CaJ mice, and cre-dependent inhibitory DREADDS (pAAV.hsyn.DIO.hM4D(Gi).mcherry; 1.2×10^{13} GC/mL) in LC. We waited for the mice to recover for a week and paired them with a mate. When the pups were born, we recorded interactions from PND0-PND3. Each day, we habituated the mice to a soundproof box in the home cage with the pups for 10 min. We then injected either saline (0.9% NaCl) or clozapine (0.1 mg/kg) (HelloBio, Inc.) dissolved in saline and waited 20 min. Then, we recorded interactions with pups for 10 min and quantified the mice latency to retrieve the pups back to the nest.

QUANTIFICATION AND STATISTICAL ANALYSIS

All the statistical tests (except for brain-wide c-fos mapping; see next section) were performed using GraphPad Prism 9. All statistical data and N values for the number of animals can be found in the figure legends and Table S4. Data are reported as mean ± SEM.

Statistical analysis for *c-fos* mapping

Statistical comparisons between different groups were run based on either ROIs or evenly spaced voxels. Voxels are overlapping 3D spheres with 100 μm diameter each and spaced 20 μm apart from each other. The cell counts at a given location, Y, are assumed to follow a negative binomial distribution whose mean is linearly related to one or more experimental conditions, X: $E[Y] = \alpha + \beta X$. For example, when testing an experimental group versus a control group, the X is a single column showing the categorical classification of mouse sample to group id, i.e. 0 for the control group and 1 for the experimental group.[65,66] We found the maximum likelihood coefficients α and β through iterative reweighted least squares, obtaining estimates for sample standard deviations in the process,

from which we obtained the significance of the β coefficient. A significant β means the group status is related to the cell count intensity at the specified location. The z-values in our summary tables correspond to this β coefficient normalized by its sample standard deviation, which under the null hypothesis of no group effect, has an asymptotic standard normal distribution. The p values give us the probability of obtaining a β coefficient as extreme as the one observed by chance assuming this null hypothesis is true. In the case of three (or more) groups, we utilize Tukey's Honest Significance test to adjust the p values of the group factor coefficients to control for multiple comparisons: group1v2, group1v3 and group2v3. To account for multiple comparisons across all voxel/ROI locations, we thresholded the p values and reported false discovery rates with the Benjamini-Hochberg procedure.[67] In contrast to correcting for type I error rates, this method controls the number of false positives among the tests that have been deemed significant.